THE UNIVERSITY OF ALBERTA

A NUMERICAL STUDY OF THE PERTURBATION OF ALTERNATING GEOMAGNETIC FIELDS NEAR ISLAND AND COASTLINE STRUCTURES

by

© LAURENCE RICHARD LINES

A THESIS

SUBMITTED TO THE FACULTY OF GRADUATE STUDIES AND RESEARCH

IN PARTIAL FULFILLMENT OF THE REQUIREMENTS FOR THE DEGREE

OF MASTER OF SCIENCE

IN

GEOPHYSICS

DEPARTMENT OF PHYSICS

EDMONTON, ALBERTA

SPRING 1973

ABSTRACT

Electromagnetic induction in the earth is studied by numerical techniques.

The perturbation of alternating geomagnetic fields by two-dimensional structures is investigated by a finite difference method. Calculations of the amplitudes and phases of the surface electric and magnetic field components are given for three two-dimensional E-polarization coastline models. The results show the effects of the electric currents in the ocean and in the mantle. The two-dimensional results indicate the similarities between the coastal effect due to the ocean alone and the coastal effect due to the ocean and the mantle. Two different frequencies of the sinusoidally time-varying electromagnetic fields are used and so skin effects are shown in the results.

A technique for modeling geomagnetic perturbations by three-dimensional structures is developed. This technique involves solving Maxwell's equations in finite difference form by using the Gauss-Seidel iterative method over a grid of variable dimensions. Two different three-dimensional island structures are studied for sinusoidally time-varying source fields of three different frequencies. Contour plots of the amplitudes of the $\underline{E}$ and $\underline{H}$ components over the surface of the conducting region

are compared near the islands. Profiles of the amplitudes and phases of the $\underline{E}$ and $\underline{H}$ components over the surface of the conducting region are compared near the islands. Skin effects are shown from a comparison of amplitude profiles for different source frequencies. The distortions of the electric and magnetic fields by the two types of island structures are illustrated and compared in the results.

The numerical method for investigating the perturbation of alternating geomagnetic fields by imbedded three-dimensional conductivity inhomogeneities in a layered earth is extended to include certain models in which vertical discontinuities may extend to the grid boundaries. A model of an island near a coastline in which the electric field vector, $\underline{E}$, is parallel to the coastline at large distances from the island is considered. Amplitude contours and profiles of the electric and magnetic field components and three-dimensional plots of the phases of the field components are given. The results indicate how islands perturb the geomagnetic effects of coastlines.

ACKNOWLEDGEMENTS

I wish to express my sincere gratitude and appreciation to my supervisor, Dr. F.W. Jones for his encouragement, guidance and assistance throughout the course of this study.

I am indebted to Mr. L.J. Pascoe and Mr. B. Ainslie for their invaluable assistance in computer programming.

I thank Dr. E. Nyland and Mr. L. Lewis for their assistance in using the GRID (Graphical Remote Interactive Display) at the University of Alberta.

I also wish to thank Prof. A.T. Price, Dr. D.I. Gough, Dr. D. Rankin, and Mr. R. Hibbs for their helpful advice and discussions on geophysical electromagnetic problems.

Finally, I would like to sincerely thank the National Research Council of Canada for financial assistance in the form of a scholarship.

TABLE OF CONTENTS

LIST OF TABLES

LIST OF FIGURES

CHAPTER 1

INTRODUCTION

1.1 General Outline of the Study

Time-varying electromagnetic fields outside the solid earth induce electric currents within conducting structures in the earth. One geophysical problem which has received much attention in recent years is that of determining the effect of these currents on the electric and magnetic fields at the surface of the earth.

Some conducting structures of interest are essentially two-dimensional in nature, and various methods have been developed to model the electromagnetic effects of such structures. One of these methods is the finite difference technique of Jones and Price (1970). A study of some features of the basic two-dimensional coastal structure problem has been made as part of the thesis work described here. In this study, the basic method of Jones and Price (1970), with further extensions by Jones and Pascoe (1971), Pascoe and Jones (1972), and Jones and Ainslie (1972) is used. One paper which describes this aspect of the thesis work has been written (Lines et al., 1972).

Although the study of electromagnetic induction effects caused by two-dimensional structures has been

of great value, geomagnetic anomalies due to some structures exhibit a clear three-dimensional nature. An island is one example of a structure whose induction effects must be analysed by three-dimensional methods. The effects of islands on time-varying geomagnetic fields are examined by a three-dimensional method in this thesis. A numerical method originally developed by Jones and Pascoe (1972) has been extended and applied to this problem. A paper (Lines and Jones, 1972a) which describes the results and compares them qualitatively with observations (Mason, 1963) has been written.

Another structure of geophysical interest in studies such as these is that of an island near a coastline. The geomagnetic effects of this type of structure are examined in this work by using a combination of two-dimensional and three-dimensional numerical techniques. The results of this study are given in this thesis and are presented in a third paper (Lines and Jones, 1972b).

In the following discussion, the basic mathematical problems of electromagnetic induction are outlined. Various two-dimensional numerical methods are mentioned with emphasis on the finite difference method. Also, a numerical method for obtaining solutions for electromagnetic induction in three-dimensional structures is given.

1.2 Mathematical Formulation of the Electromagnetic Induction Problem

1.2.1 Equations and Boundary Conditions

To investigate the electromagnetic induction of currents in a stationary, conducting medium, the basic problem is the solution of Maxwell's equations which may be written in electromagnetic units as:

$$\nabla.\underline{D} = 4\pi\rho \ , \tag{1.1}$$

$$\nabla\times\underline{H} = 4\pi\underline{J} + \frac{\partial\underline{D}}{\partial t} \ , \tag{1.2}$$

$$\nabla\times\underline{E} = -\frac{\partial\underline{B}}{\partial t} \ , \tag{1.3}$$

$$\nabla.\underline{B} = 0 \ . \tag{1.4}$$

For conductors in which Ohm's law is satisfied, the current density ($\underline{J}$) is related to the electric field ($\underline{E}$) by

$$\underline{J} = \sigma\underline{E} \ , \tag{1.5}$$

where σ is the conductivity of the conductor.

The electric displacement ($\underline{D}$) is related to the electric field intensity ($\underline{E}$) by

$$\underline{D} = \varepsilon\underline{E} \ , \tag{1.6}$$

where ε is the electric permittivity.

The magnetic induction vector ($\underline{B}$) is related to the magnetic field intensity ($\underline{H}$) by

$$\underline{B} = \mu \underline{H} \quad , \tag{1.7}$$

where μ is the magnetic permeability.

It is assumed in the models here that all materials are non-magnetic, so that $\mu = \mu_o = 1$ in electromagnetic units and $\underline{B} = \underline{H}$.

From the Maxwell equation which describes Faraday's induction law (1.3), it is clear that if there exists a time-varying magnetic field near a conducting surface, an electromotive force will be created within the conductor which will cause electric currents to flow. Also, the Maxwell equation describing Ampere's law (1.2) shows that these induced currents flowing in the conductor contribute to the magnetic field observed at the surface of the conductor.

In all cases considered in the following, the conductor represents the earth, and the time-varying inducing magnetic field originates from some source external to the solid earth.

The time variation of the fields studied is assumed to be sinusoidal so that

$$\underline{E}(x,y,z,t) = \underline{E}(x,y,z)\, e^{i\omega t} \tag{1.8}$$

and

$$\underline{H}(x,y,z,t) = \underline{H}(x,y,z)\, e^{i\omega t} \quad , \tag{1.9}$$

where $\omega = 2\pi/T$ and T is the period of oscillation.

In all models considered the displacement current term, $\partial \underline{D}/\partial t$, is neglected. The conditions for which displacement currents may be neglected are explained by Garland (1971). If we consider equation (1.2), and if L and T are the characteristic length and time of variation of the electromagnetic field, then $\partial \underline{D}/\partial t$ is of order $\varepsilon \underline{E}/T = \varepsilon\mu HL/T^2$, and $\nabla \times \underline{H}$ is of order $\underline{H}/L$. Hence, $\partial \underline{D}/\partial t$ is negligible compared to $\nabla \times \underline{H}$ whenever $T >> (\varepsilon\mu)^{\frac{1}{2}} L$. Price (1967) points out that for L of order 4×10^9 cm and $(\varepsilon\mu)^{\frac{1}{2}}$ of order C^{-1}, $\partial \underline{D}/\partial t$ is negligible if $T >> 0.1$ sec. All values of T used here are one minute or larger, so that $\partial \underline{D}/\partial t$ may be neglected and equation (1.2) becomes

$$\nabla \times \underline{H} = 4\pi \underline{J} \quad . \tag{1.10}$$

Although the magnetic effects of $\partial \underline{D}/\partial t$ are negligible, this does not imply that the physical effects of $\underline{D}$ can be ignored.

If displacement currents are neglected, and if it is assumed that the electric and magnetic fields have a sinusoidal time variation, then equations (1.2) and (1.3) may be written as two coupled equations in $\underline{E}$ and $\underline{H}$:

$$\nabla \times \underline{H} = 4\pi\sigma \underline{E} \quad , \tag{1.11}$$

$$\nabla \times \underline{E} = -i\omega \underline{H} \quad . \tag{1.12}$$

By taking the divergence of (1.11), we see that $\nabla . \underline{E}$ vanishes in regions of uniform conductivity which implies that no charge distributions exist in such

regions. Also, by taking the divergence of (1.12), we see that the divergence of $\underline{H}$ must vanish everywhere.

By taking the curl of (1.12) and substituting for $\nabla\times\underline{H}$ from (1.11), we obtain the following equation in $\underline{E}$:

$$\nabla(\nabla.\underline{E}) - \nabla^2\underline{E} = -i4\pi\sigma\omega\underline{E} \ . \qquad (1.13)$$

This is the equation which must be solved for $\underline{E}$ in all regions.

In a non-magnetic material the tangential components of $\underline{E}$ and $\underline{H}$ and the normal component of $\underline{H}$ are all continuous across any interface. If displacement currents are neglected, the normal component of $\underline{J}$ is continuous across any boundary. The normal component of $\underline{D}$ is discontinuous across an interface only if surface charges are present on the interface.

1.2.2 The Global and Local Problems

A comprehensive review of the types of mathematical problems involved in geophysical electromagnetic induction studies was given by Price (1964). Price divides the problems of induction into two main types, global problems and local problems.

In global problems, we are concerned with electromagnetic induction over the entire earth, and the earth is treated as a spherical conductor in which the

conductivity, σ, is a smoothed function of the spherical coordinates (r,θ,ϕ). Only large scale variations in conductivity are considered. Lahiri and Price (1939) gave solutions for induction in a conducting sphere in which the conductivity was proportional to r^{-m}, where m is an integer.

In local problems, the sphericity of the earth is neglected, and the earth is treated as a semi-infinite conductor with a plane surface. In this type of problem, the inducing field is usually of global dimensions, but conductivity distributions are quite localized and we are usually interested in conductivity variations over distances of the order of 100 km or less. Wait (1962) showed that for periods of the order of 10^3 sec the use of a semi-infinite conductor with plane boundaries is a good approximation to the spherical earth. Srivistava (1966) stated that for conductivities from 10^{-2} to 10^{-3} mho m^{-1} (or 10^{-13} to 10^{-14} emu) the effect of the earth's curvature may be neglected for source periods of less than a day. Also, Price (1967) points out that plane earth models are generally satisfactory for the study of local perturbation problems.

Therefore, conductivity structures for the local problem are generally defined in Cartesian coordinates (x,y,z). In the following discussion, a non-uniform conductor occupies the half-space $z > 0$.

The theory for induction in a semi-infinite conductor with a plane boundary for a given arbitrary source was outlined by Price (1950). Cagniard (1953), in his classic paper on the magnetotelluric method, considered induction in a horizontally layered earth due to plane electromagnetic waves. This paper by Cagniard generated discussions by Wait (1954) and Price (1962) on the validity of Cagniard's source field assumptions. Recently, Hibbs (1972) has given a review of source studies, and has given results for an aperiodic, spatially time varying source.

In the present study of induction in three-dimensional structures, a uniform inducing source is assumed for induction in imbedded structures.

Price (1964) explains that the local problem may be considered as a perturbation problem. While the strength of induced currents in the local problem is determined by the geometry and conductivity of a conductor over a region of large dimensions, Price points out that the induced field in an anomalous region is determined by the local redistribution of an extended current system. This current redistribution is caused by abrupt local changes in conductivity. It is important to note that redistributions of current flow at depth are not entirely disturbances of steady current flow, but also involve skin effects due to the fact that the currents are alternating.

1.2.3 The Skin Effect

In a region of uniform conductivity, the electric field vector satisfies a diffusion equation in which $\underline{E}$ varies only with depth:

$$\frac{d^2\underline{E}}{dz^2} = i4\pi\sigma\omega\underline{E} \quad . \tag{1.14}$$

This equation, which is a simplified form of (1.13), is sometimes referred to as the equation in $\underline{E}$ for a one-dimensional earth.

From (1.11) it is evident that E_z vanishes if there are no lateral variations in H_x or H_y. If we choose $\underline{E}$ to be in the x direction, then equation (1.14) becomes

$$\frac{d^2E_x}{dz^2} = i4\pi\sigma\omega E_x \quad . \tag{1.15}$$

The general solution of (1.15) is given by:

$$E_x = A\, e^{-\sqrt{i}\eta z} + B\, e^{\sqrt{i}\eta z} \quad , \tag{1.16}$$

where

$$\eta^2 = 4\pi\sigma\omega \quad .$$

In order for E_x to remain finite as $z \to \infty$, we must set B equal to zero. Therefore, E_x has an attenuation factor of

$$e^{-\frac{1}{\sqrt{2}}\eta z} \quad .$$

The electric field (and also the current density) is attenuated to e^{-1} of its surface value at a depth $\sqrt{2}\eta^{-1}$ or $(2\pi\sigma\omega)^{-\frac{1}{2}}$. This depth is known as the skin depth, and is a measure of the depth of penetration of induced currents. It is important to note that the skin depth is inversely proportional to the square root of both the conductivity and the frequency. The skin depth is important in that its value helps to determine the distribution of electric and magnetic fields at the surface of the earth in the local perturbation problem.

CHAPTER 2

TWO-DIMENSIONAL PROBLEMS IN ELECTROMAGNETIC INDUCTION

2.1 Theory of Two-Dimensional Induction Problems

In the two-dimensional problem we assume that the conductivity structure varies only with two Cartesian coordinates (x and z, say). It then follows that there is no variation of the electric and magnetic fields in the y direction, and equations (1.11) and (1.12) may then be rewritten with $\partial/\partial y \equiv 0$ as:

$$\frac{\partial H_y}{\partial z} = -4\pi\sigma E_x \tag{2.1}$$

$$\frac{\partial H_x}{\partial z} - \frac{\partial H_z}{\partial x} = 4\pi\sigma E_y \tag{2.2}$$

$$\frac{\partial H_y}{\partial x} = 4\pi\sigma E_z \tag{2.3}$$

$$\frac{\partial E_y}{\partial z} = i\omega H_x \tag{2.4}$$

$$\frac{\partial E_x}{\partial z} - \frac{\partial E_z}{\partial x} = -i\omega H_y \tag{2.5}$$

$$\frac{\partial E_y}{\partial x} = -i\omega H_z \quad . \tag{2.6}$$

The above set of Maxwell's equations in two dimensions may be divided into two separate sets of equations

which can be solved independently. One set includes equations (2.2), (2.4) and (2.6) in which only E_y, H_x and H_z are involved. This set corresponds to the E-polarization case. By combining these equations we obtain the following equation in E_y:

$$\frac{\partial^2 E_y}{\partial x^2} + \frac{\partial^2 E_y}{\partial z^2} = i\eta^2 E_y \quad , \tag{2.7}$$

where

$$\eta^2 = 4\pi\sigma\omega .$$

Since $\underline{E}$ is totally in the y direction in the E-polarization case, the electric field vector is parallel to the strike of any two-dimensional conductivity discontinuities in the x-z plane. The boundary conditions for the E-polarization case will be discussed in detail later.

The second set of equations includes (2.1), (2.3), and (2.5), and involves only E_x, E_z, and H_y. This set of equations corresponds to the H-polarization case, and by eliminating E_x and E_z, we obtain:

$$\frac{\partial^2 H_y}{\partial x^2} + \frac{\partial^2 H_y}{\partial z^2} = i\eta^2 H_y \quad . \tag{2.8}$$

In the region outside the conductor where $\sigma = 0$, equations (2.1) and (2.3) show that H_y is independent

of x and z, and so in the H-polarization case H_y is uniform above the surface of the conductor and is not affected by abrupt lateral discontinuities within the conductor.

2.2 Analytical Solutions of Two-Dimensional Problems

Following Cagniard's investigation (Cagniard, 1953) of a horizontally stratified or one-dimensional earth model, the effects of lateral inhomogeneities in two-dimensional conductivity models were considered by several authors.

D'Erceville and Kunetz (1962) studied the effect of lateral conductivity variations in the earth's interior by considering the effect of a vertical fault on the earth's electromagnetic field for the H-polarization case. Also, Rankin (1962) gave an analytical solution for the magnetotelluric effect of a dike for the H-polarization case.

Weaver (1963) obtained analytical solutions for the E and H polarization fields of an infinite conducting half-space consisting of two quarter-spaces of different conductivities. In the E-polarization case, Weaver used an approximate boundary condition which assumed that the horizontal magnetic field along the surface of the conducting region was constant. Recently, Weaver and Thomson (1972) have used a perturbation

technique originally proposed by Mann (1970) to obtain approximate analytic solutions for a periodic line current above a non-uniform earth. Also, Weaver and Thomson (1972) have obtained limiting expressions for the fields for the case when the height and magnitude of the line current approach infinity in such a way that the inducing field near the earth becomes uniform and finite.

Analytic solutions to geophysical electromagnetic problems usually apply to special types of conductivity configurations. In obtaining solutions for conducting structures with arbitrary shapes, it is often necessary to use numerical techniques.

2.3 Numerical Techniques used in the Two-Dimensional Problem

2.3.1 Outline of Various Numerical Techniques

In recent years several pure numerical techniques (that is, methods in which the equations are evaluated from the beginning by numerical means) have been devised to obtain solutions for various two-dimensional problems. A brief review of these techniques has been given by Jones (1972).

In these numerical methods a mesh of grid points is superimposed over the conductivity configuration so

that a conducting structure is represented by a number of conducting cells which are electrically homogeneous.

In the finite element method a solution is obtained by numerically minimizing the total electromagnetic energy of all the conducting cells. The finite element method as applied to electromagnetic problems has been described by Coggon (1971). Recently, Reddy and Rankin (1972) have used the finite element method in finding the magnetotelluric response of a two-dimensional sloping contact.

Another numerical method which has been employed for use in two-dimensional problems is the transmission line analogy. This method employs the similarity in form between Maxwell's equations governing the orthogonal components of $\underline{E}$ and $\underline{H}$ and the transmission equations governing current and voltage over a transmission surface. This method is described in detail by Wright (1969).

A third numerical technique, the finite difference method, which is the method used in this thesis to determine solutions to the local perturbation problem, is described in detail in the following section.

2.3.2 The Finite Difference Method

The finite difference technique in the study of electromagnetic induction problems was first used by Neves (1957). Also, Latka (1966), and Patrick and Bostick (1969) have used this method. Jones and Price (1970)

employed the finite difference technique to determine both the E-polarization and H-polarization fields associated with lateral discontinuities in conductivity.

The equations for both the E-polarization and H-polarization cases, as given by (2.7) and (2.8), have the form

$$\frac{\partial^2 F}{\partial x^2} + \frac{\partial^2 F}{\partial z^2} = i\eta^2 F \quad , \tag{2.9}$$

where $F = E_y$ in the E-polarization case, and $F = H_y$ in the H-polarization case.

If we set $F = f + ig$ and equate the real and imaginary parts of (2.9) we obtain:

$$\frac{\partial^2 f}{\partial x^2} + \frac{\partial^2 f}{\partial z^2} = -\eta^2 g \quad , \tag{2.10}$$

and

$$\frac{\partial^2 g}{\partial x^2} + \frac{\partial^2 g}{\partial z^2} = \eta^2 f \quad . \tag{2.11}$$

Equations (2.10) and (2.11) must be satisfied at each point in a grid of mesh points. The numerical formulation for the solution of these equations is described by Jones and Pascoe (1971). Figure 1, taken from Jones and Pascoe (1971), shows the notation used for grid points. To obtain a set of finite difference equations Jones and Pascoe (1971) used a Taylor series

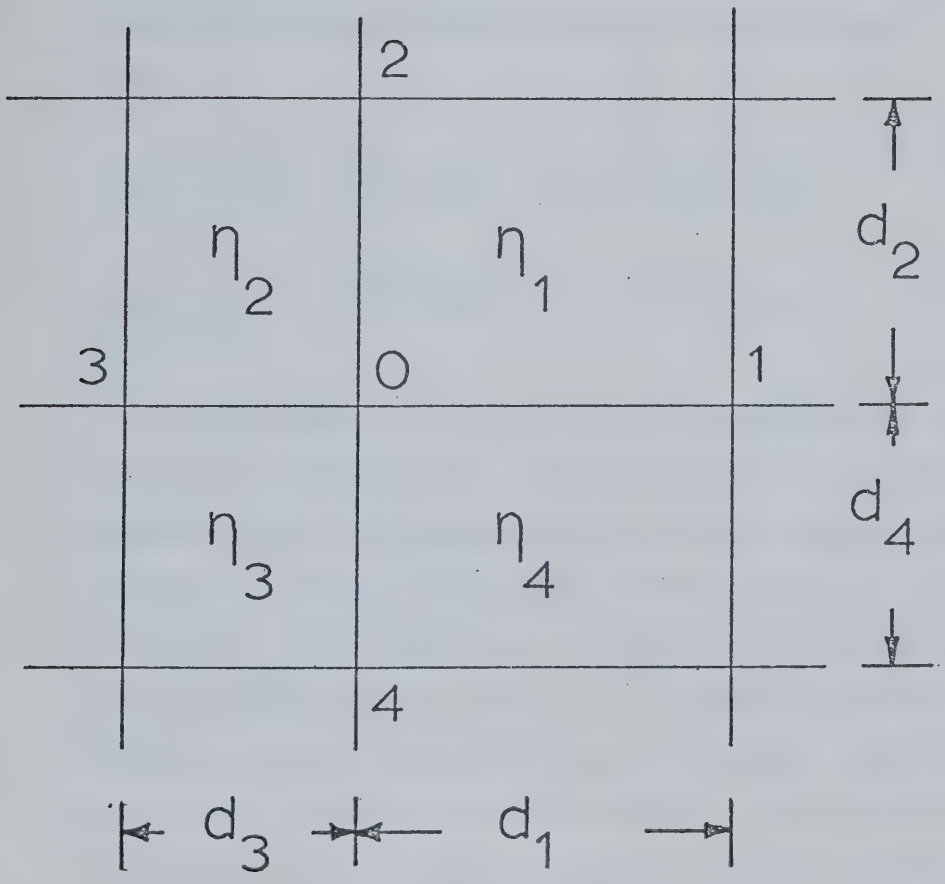

Fig. 1. Two-dimensional notation used for grid points, dimensions, and conductivities surrounding a point '0'. (After Jones and Pascoe, 1971).

approximation. The first derivatives in this approximation were replaced by central difference formulae. A pair of finite difference equations which must be satisfied at each interior point of the grid was obtained:

$$f_o\left(\sum_{i=1}^{4} \frac{1}{d_i^2}\right) - \eta^2 g_o = f_1 D_1 + f_2 D_2 + f_3 D_3 + f_4 D_4 \qquad (2.12)$$

$$g_o\left(\sum_{i=1}^{4} \frac{1}{d_i^2}\right) + \eta^2 f_o = g_1 D_1 + g_2 D_2 + g_3 D_3 + g_4 D_4 \quad . \qquad (2.13)$$

The values D_1, D_2, D_3 and D_4 are constants related to the grid dimensions, and are described by Jones and Pascoe (1971). The quantities f_i and g_i represent the values of f and g at the grid points (i=0,1,2,3,4) shown in Fig. 1. The quantities d_i (i=1,2,3,4) represent the grid intervals shown in Fig. 1. To write the above finite difference equations for each region requires the use of 'fictitious' values (Smith, 1969), which are subsequently eliminated by imposing internal boundary conditions on $\underline{E}$ and $\underline{H}$. These 'fictitious' values refer to values of f and g for points not included in the particular conducting region being considered, and the elimination of these values by application of the boundary conditions is described in detail by Jones and Pascoe (1971).

The finite difference method as developed by Jones and Price (1970), Jones and Pascoe (1971) and Pascoe and Jones (1972) is used in this thesis to analyse the E-polarization coastal problem.

2.3.3 Boundary Conditions for the E-Polarization Case

Originally, the finite difference methods of Jones and Pascoe (1971) were used to model long cylinders of arbitrary shape imbedded in a region of uniform conductivity. The method was later generalized by Pascoe and Jones (1972) so that the fields associated with conductivity inhomogeneities imbedded in layered structures could be determined. Moreover, in the later generalization, provision was made for situations in which the layered structures for such models need not be identical at the left and right boundaries of the grid. A diagram of the grid boundary and coordinate system is given in Fig. 2.

Since the left and right hand sides of the model shown in Fig. 2 consist of horizontal layers and are far removed from lateral discontinuites, $\partial E_y/\partial x = 0$ for the extreme values of x. The E-polarization equations at the boundaries then reduce to:

$$\frac{\partial^2 E_y}{\partial z^2} = i\eta^2 E_y \quad . \tag{2.14}$$

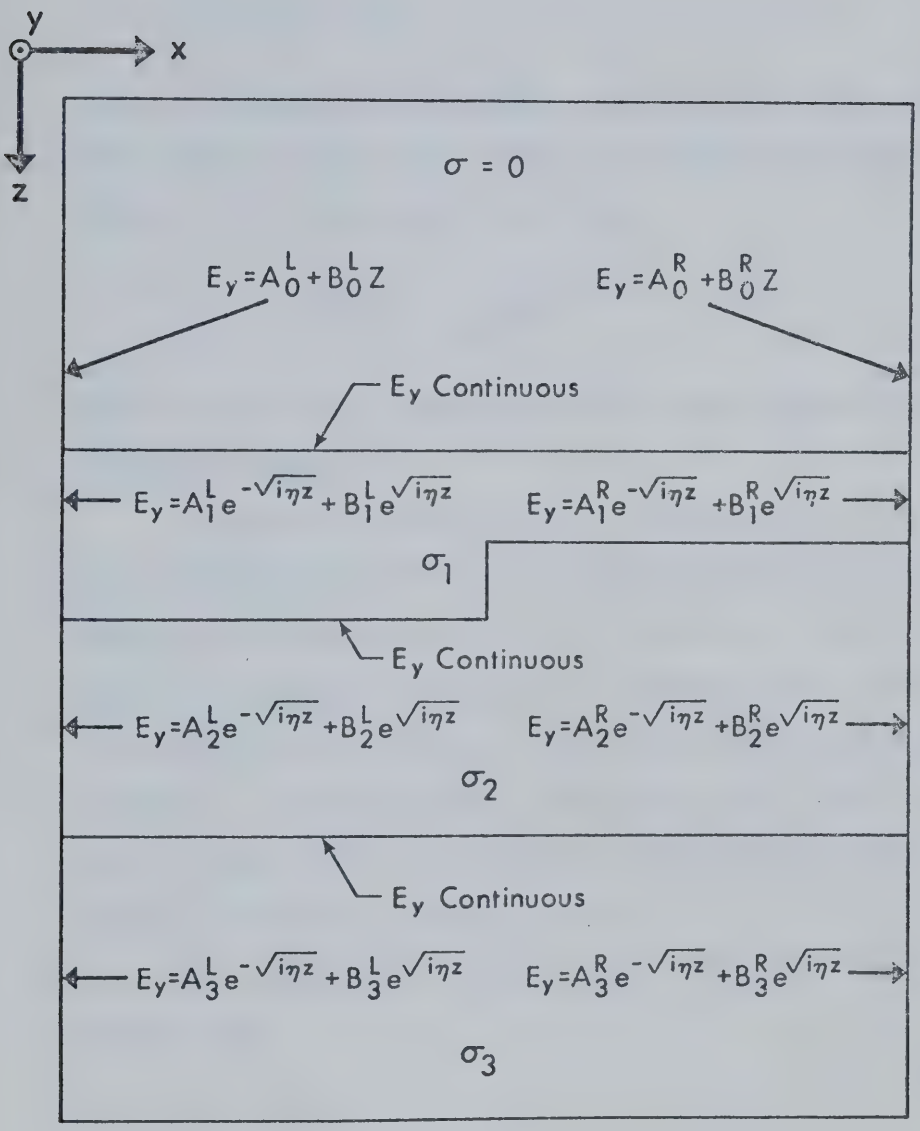

Fig. 2. Boundary conditions on E_y for the E-polarization case.

Above the surface of the conductor, where $\eta = 0$,

$$E_y = A_o + B_o z \quad , \tag{2.15}$$

where A_o and B_o are constants. At the left and right hand sides of the grid within the conducting region (where $\eta \neq 0$), E_y takes the form:

$$E_y = A\, e^{-\sqrt{i}\eta z} + B\, e^{\sqrt{i}\eta z} \quad , \tag{2.16}$$

where A and B are constants whose values depend on the conducting layer.

In order to ensure that E_y remains finite as $z \to \infty$, B is set equal to zero in the deepest conducting layer (which is the lowest grid row). Values of A and B in the rows above are determined by imposing the continuity conditions on E_y and H_x at the layer interfaces along the boundary. In this manner, the values of E_y are set for the left and right hand sides of the general model, an example of which is shown in Fig. 2.

For the E-polarization case, Jones and Price (1970) showed that

$$H_{o1} = H_{o2} \quad , \tag{2.17}$$

where H_{o1} and H_{o2} are the surface values of H_x at the extreme left and right hand sides of the grid respectively. This boundary condition on the surface values of H_x allows evaluation of the surface values of E_y for the left

and right hand sides of the grid. After the surface values of E_y at the external grid boundaries are determined, all other values of E_y on the sides of the grid are adjusted accordingly. The initial values of E_y at all internal grid points are given by linear interpolation between the values of E_y at the left and right hand boundaries of the grid. These values of E_y are used as initial values in the Gauss-Seidel iterative process, which is used to obtain solutions for E_y throughout the entire grid.

2.4 Two-Dimensional Numerical Methods Applied to the Coastal Problem

2.4.1 The Coastal Effect

The effect of a coastline on surface geomagnetic variations has generated much interest in recent years. The magnetic field components near coastlines have generally shown anomalously large variations in the amplitude of the H_z component. Schmucker (1964) made a detailed study of the variations in the D, H and Z magnetic components along profiles running transverse to the California coast, and suggested that the coastal anomaly in Z (or H_z) may be caused by the edge-effect of the Pacific Ocean. Rikitake (1964) suggested that the major cause of the anomalous behaviour of the vertical magnetic

component near the coast of Japan was due to the complicated mantle structure beneath Japan. Roden (1964) studied the effect of the Pacific Ocean on magnetic variations in Japan by use of an analogue model and theoretical calculations, and suggested that currents induced in the Pacific Ocean contribute to the anomalous behaviour of the magnetic variation fields in Japan.

By using seismic and magnetic data, Lambert and Caner (1965) investigated the mantle structure beneath the British Columbia coastline. Also, Dosso (1966) has used analogue models of different coastal structures, and has examined the behaviour of the phases and amplitudes of the surface $\underline{E}$ and $\underline{H}$ components for profiles running transverse to the coastlines.

Parkinson (1964), in a paper on the coastal effect in Australia, stated that the geomagnetic effect of currents induced in the ocean could not entirely explain the coastal effect. It is apparent that there is a contribution to the coastal effect caused by a difference in mantle structure beneath the ocean and continental regions, as well as a contribution due to currents induced in the oceans.

Cox et al. (1970) considered coastal effects for the two-dimensional $\underline{E}$ and $\underline{H}$ polarization cases. The H-polarization case corresponds to a situation in which the magnetic field is parallel to the coastline, and the

E-polarization case occurs when the electric field is parallel to the coastline. For the E-polarization case, Cox et al. (1970) predicted an increase in electric current strength near the edge of the ocean which would cause an increase in the surface tangential component of the magnetic field near the coastline. Also, they suggested that the H_z increase near the coastline is due to an increased concentration of electric currents at the edge of the ocean, caused by the mutual repulsion of current lines in the highly conducting ocean. Furthermore, they pointed out that an increase in the vertical magnetic component can be caused by currents in the mantle beneath the coastline.

In the following discussion, we are interested in determining the electromagnetic coastal effects of currents in the mantle and ocean for the E-polarization case. The E-polarization equation was solved by use of the computer programs developed by Jones and Pascoe (1971), and Pascoe and Jones (1972). In addition to these programs, a "folding-in" technique developed by Jones and Ainslie (1972) was applied to better deal with these models which have high conductivity contrasts. The results of this study are included in the following section and a paper has been written (Lines et al., 1972) in which this work is described.

2.4.2 Description of the Models

The three different structures studied are shown in Fig. 3. Model 1 is a coastal model which includes only ocean and crustal structure. The electric and magnetic fields for this model will show that part of the coastal effect which is caused by oceanic electric currents. Also, besides this local effect due to the lateral discontinuity at $x = 0$, the effect of the difference in conductivity structure at $x = +\infty$ and $-\infty$ will be shown. In model 2, the effect of the mantle structure is investigated. In this model, the sloped mantle-crust interface is represented by a series of steps. In the actual situation, both of the characteristics represented by models 1 and 2 exist. An attempt to model the more general situation is represented in model 3, which is a combination of the structures of models 1 and 2. The conductivities of the crust, mantle and ocean with their respective skin depths for the frequencies considered are given in Table 1. The conductivity configuration for each model is defined over a variable grid. Table 2 gives the dimensions of the initial grid used. The final horizontal grid dimension (after 3 successive sets of iterations of the folding-in technique) is 1 km. The vertical grid dimensions remain constant throughout the four sets of iterations.

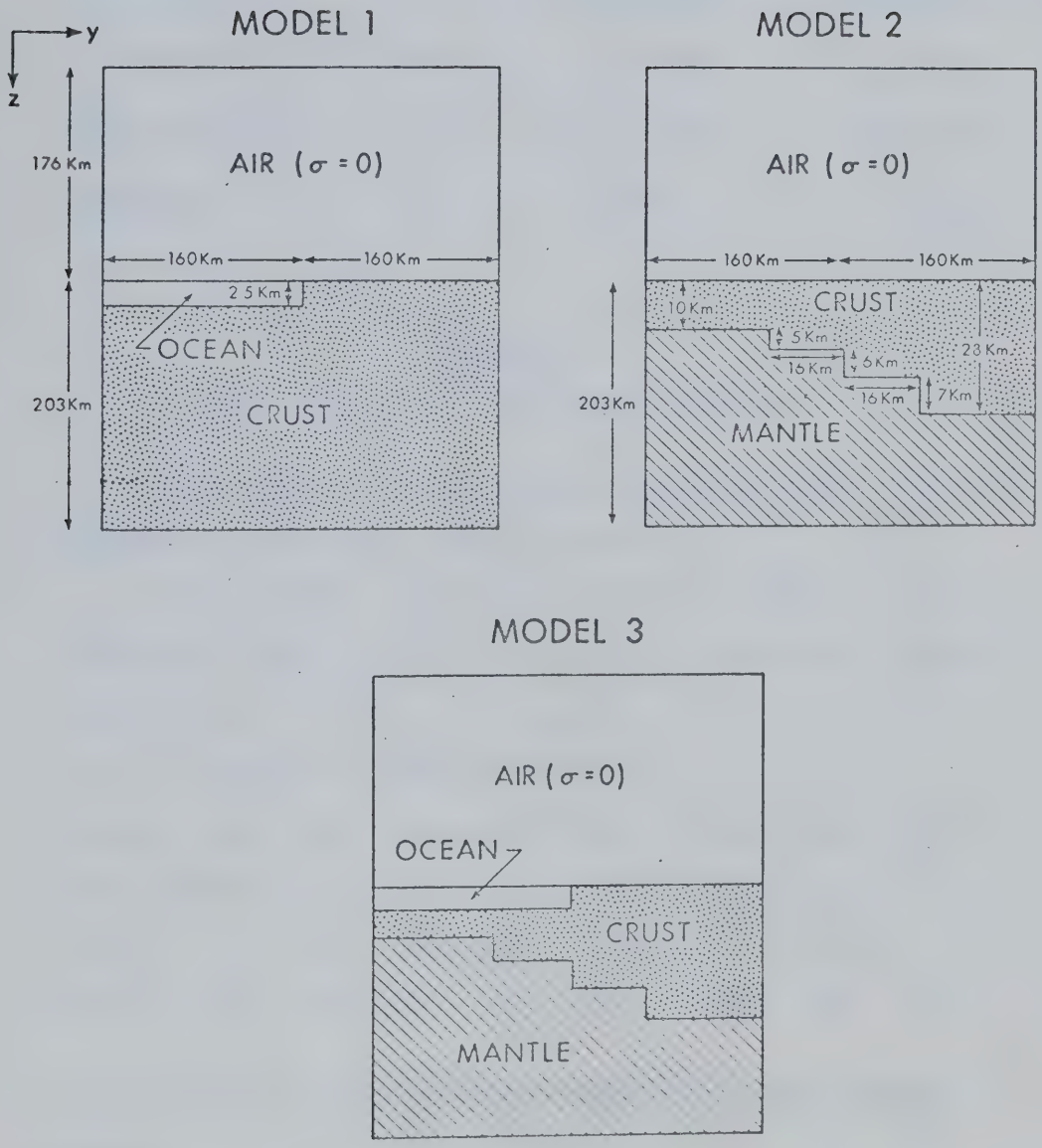

Fig. 3. The two-dimensional coastal structures considered.

Table 1

Conductivities and skin depths for the coastal models

Conductivities	Skin depths at different frequencies	
	0.03 hz	0.3 hz
σ_1 (ocean) = .8 $\times 10^{-11}$ emu	3.25 km	1.03 km
σ_2 (crust) = .21 $\times 10^{-14}$ emu	200.52 km	63.41 km
σ_3 (mantle) = .1 $\times 10^{-12}$ emu	29.06 km	9.19 km

Table 2

Grid spacing for the coastal models

Grid spacing in the variable grid network. The grid network is a 41 by 41 array of points.

y direction: Points are uniformly spaced at 8 km initially, and 1 km finally, with four successive sets of iterations.

z direction: (Spacing is in km)

70	40	30	20	13	2.5	0.5	0.5	0.5	0.5
0.5	0.5	0.5	1	1	1	1	1	1	1
1	1	1	1	1	2	2	2	2	5
5	5	5	5	5	10	20	30	40	50

(The vertical line denotes the position of the surface plane.)

Calculations of the phases and amplitudes of the electric and magnetic fields are given for all three structures for frequencies of 0.03 hz and 0.3 hz. The values of $|H_x|$ in all models are normalized so that $|H_x| = 1.0$ for the extreme values of x. The values of E_y and H_z are adjusted accordingly. This normalization allows the effect of different structures to be examined for a given source.

For a given frequency, the depth of burial of the mantle determines whether induced telluric currents flow mainly in the ocean or in the mantle. If the mantle is deeply buried beneath the more poorly conducting crust, induced currents flow mainly in the ocean, and results for model 1 provide a good approximation to observed results. On the other hand, if the mantle is shallow, induced currents flow mainly in the earth's mantle. Moreover, if the mantle is shallow beneath the ocean and deeply buried beneath the continents (as in model 3), then the coastal anomaly generated by this structure is similar to the anomaly generated by electric currents flowing mainly in the ocean.

Of primary interest is the comparison of the results of models 1 and 3. Results of model 1 show the effect of oceanic electric currents on the surface magnetic field, whereas results for model 3 show the magnetic effects of

both electric currents in the ocean and in the mantle. Model 2, which gives the effect of the mantle only, may be used to account for differences in the results of model 1 and model 3.

The amplitude of a component such as E_y is given by

$$|E_y| = [(\mathrm{Re}(E_y))^2 + (\mathrm{Im}(E_y))^2]^{\frac{1}{2}} \qquad (2.18)$$

where the time dependence $e^{i\omega t}$ has been suppressed in the expression. The phase of E_y is given by Φ, where

$$\Phi = \tan^{-1}\left(\frac{\mathrm{Im}(E_y)}{\mathrm{Re}(E_y)}\right) \quad , \quad \text{and} \quad -\pi \leq \Phi \leq \pi \quad . \qquad (2.19)$$

The spatially dependent part of a component such as E_y is given by

$$E_y(x,y,z) = |E_y| e^{i\Phi} \quad . \qquad (2.20)$$

As well as the amplitudes and phases of the electric and magnetic field components, profiles of the surface values of $|E_y/H_x|$ and $|H_z/H_x|$ are also calculated for each model.

2.4.3 Results and Discussion

Figs. 4, 5, and 6 give profiles of the amplitudes and phases of E_y, H_x and H_z for both frequencies for the three models considered. In both models 1 and 3, the

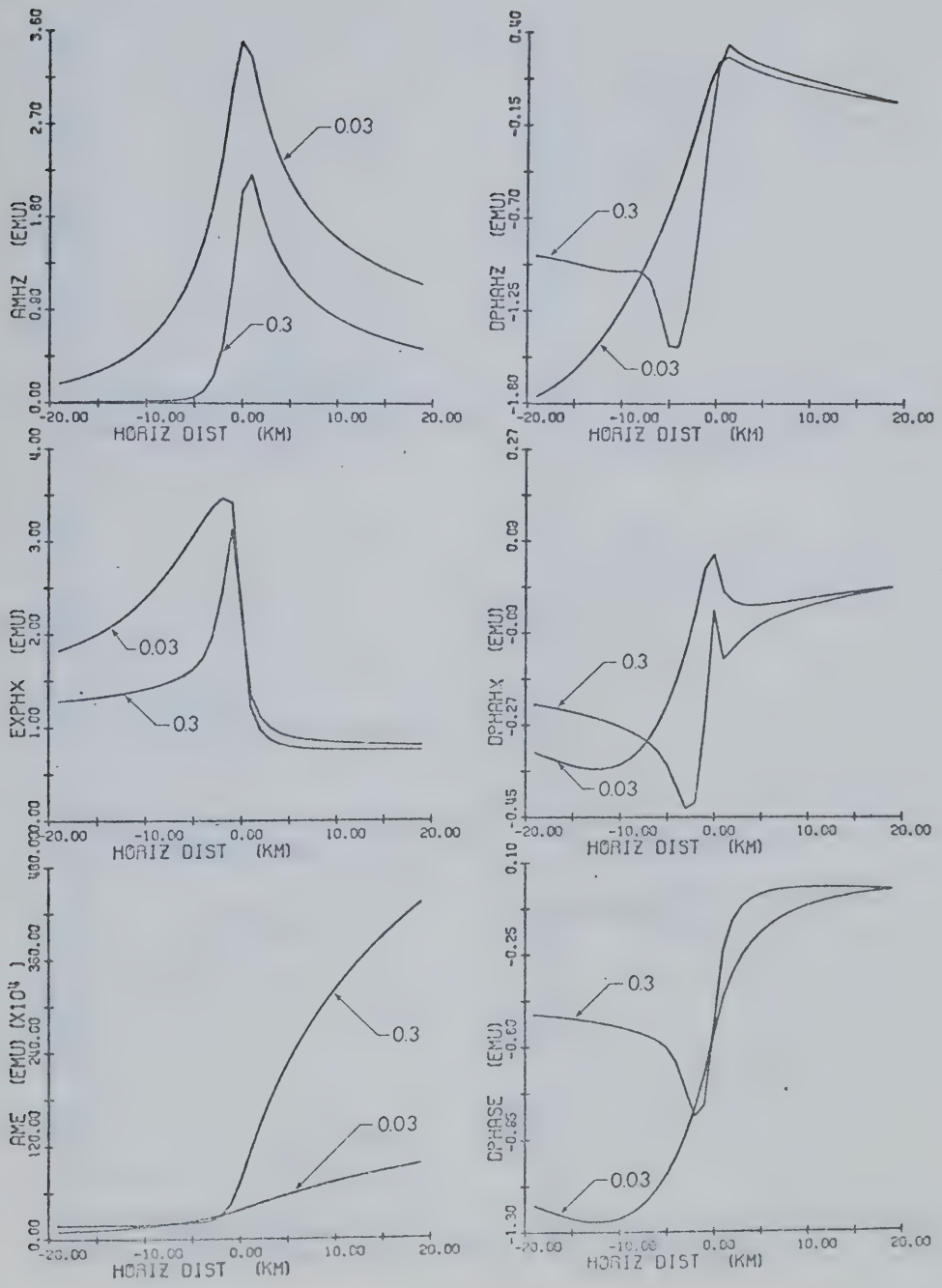

Fig. 4. The amplitude and phase profiles of E_y, H_x, and H_z for model 1. Notation used: AME = amplitude of E_y, EXPHX = amplitude of H_x, AMHZ = amplitude of H_z, DPHASE = phase of $E_y - \pi$, DPHAHX = phase of H_x, DPHAHZ = phase of H_z.

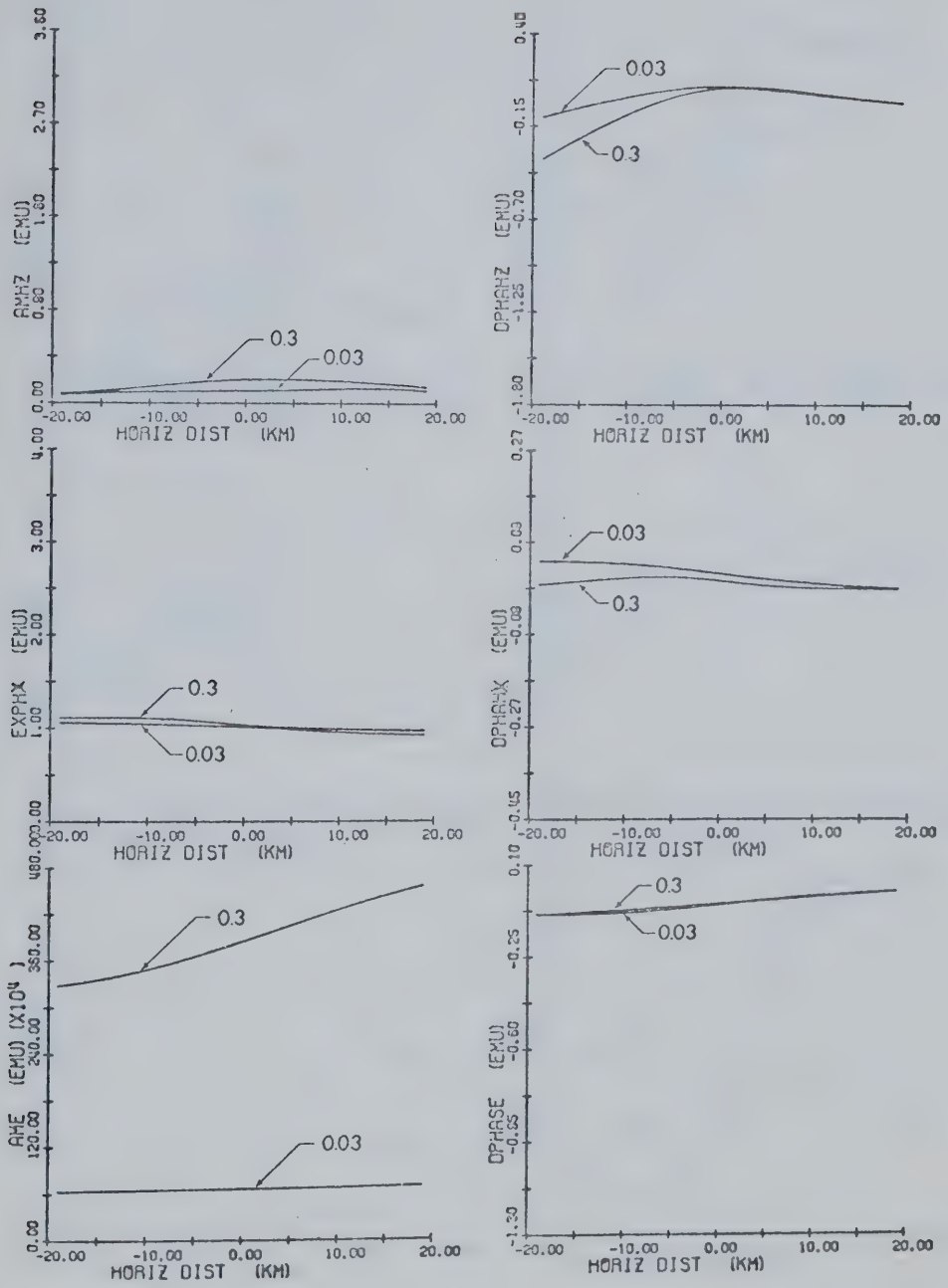

Fig. 5. The amplitude and phase profiles of E_y, H_x, and H_z for model 2. (Same notation as in Fig.4).

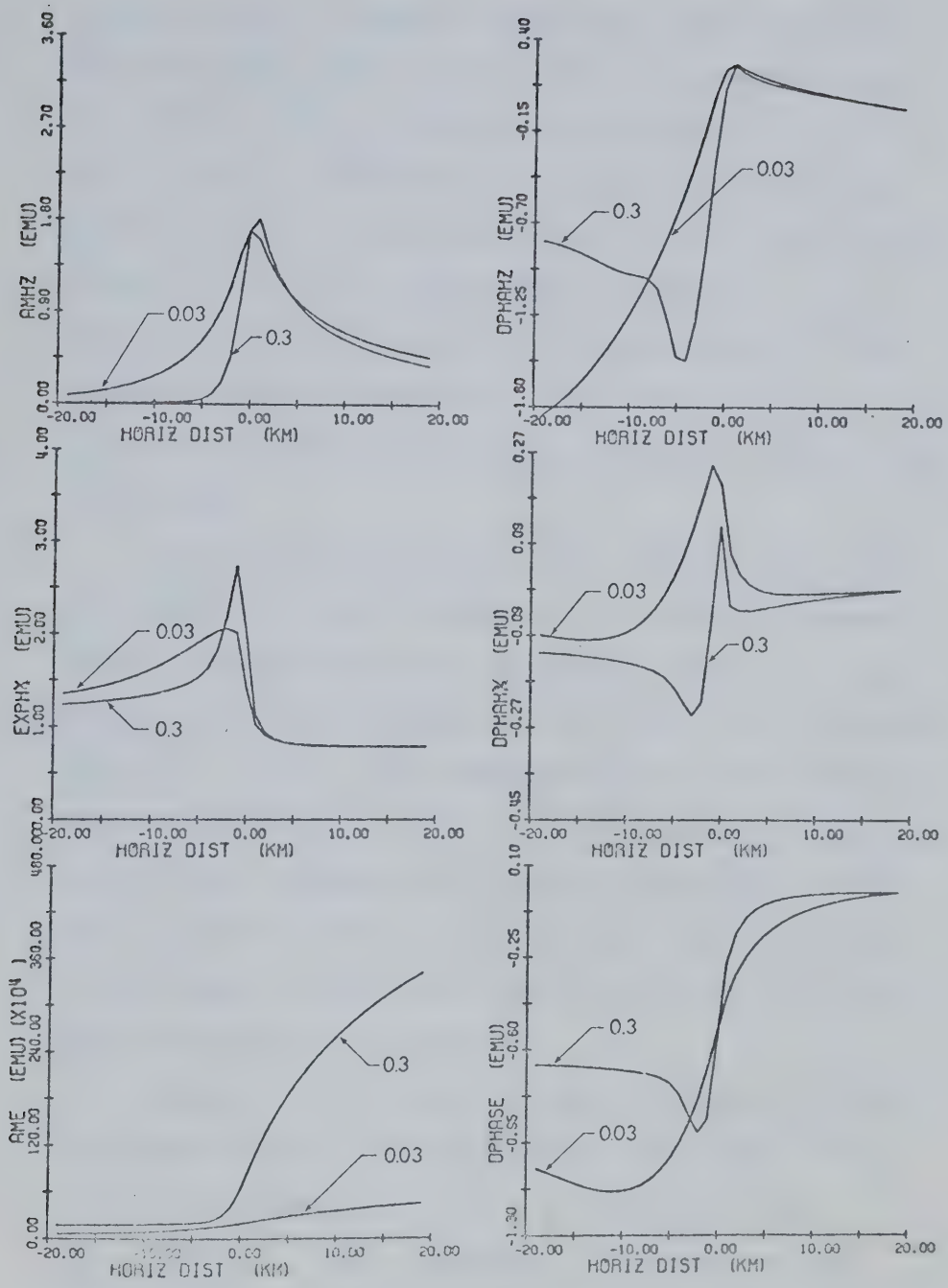

Fig. 6. The amplitude and phase profiles of E_y, H_x, and H_z for model 3. (Same notation as in Fig.4).

value of $|E_y|$ is always greater over the continents than over the ocean. This result is expected since it is due to the difference in conductivity as $y \to +\infty$ and $-\infty$, and is reflected in the boundary conditions imposed on the E-polarization solutions. This boundary condition (which is essentially a result of (2.17)) requires that the value of E_y at the surface of the medium of lower conductivity (the crust) be larger than E_y at the surface of the medium of higher conductivity (the ocean).

In both models 1 and 3, the change in $|E_y|$ over the coastline is more abrupt for the higher frequency. These sudden changes are essentially due to the skin effect. At high frequencies, the skin depth (given by $(2\pi\sigma\omega)^{-\frac{1}{2}}$) is less, and consequently the penetration of electric currents is less. For this reason, shallow conductivity features such as the continential shelf have a greater effect on the surface electric fields at the higher frequencies, and thus changes in E_y are more abrupt at the surface.

Models 1 and 3 show a sudden change in $|H_z|$ near the coastline for both frequencies considered. This increase is expected from the calculation of H_z, ($H_z = \frac{-1}{i\omega} \frac{\partial E_y}{\partial x}$). The E_y component increases as the coastline is approached from the ocean side, giving a

large value of $\partial E_y/\partial x$ near the coast, and causing an increase in $|H_z|$. A physical argument, given by Cox et al. (1970) suggests an explanation for the cause of the H_z increase in the E-polarization case. They suggest that mutual repulsion of current lines in the conducting ocean causes an increased concentration of electric currents at the edge of the ocean. As a result of Ampere's law, this increase in current strength near the coastline causes an increase in the magnitude of the vertical component of the magnetic field. A similar phenomenon occurs for currents in the mantle of model 2, as shown in Fig. 5.

The $|H_z|$ values of model 3 are lower than those of model 1. This demonstrates that magnetic fields due to currents in the mantle of model 2 do not simply add to the magnetic fields due to the oceanic electric currents in model 1 to give the magnetic field of model 3. A reduction in the $|H_z|$ values of model 3 is caused by a change in the direction of currents with depth for given instants in time. Examples of changes in the sign of currents with depth are shown in the E-polarization results of Jones and Price (1970).

An increase in electric current strength near the edge of the ocean as predicted by Cox et al. (1970) will also cause an increase in the surface tangential component of the magnetic field near the coastline. This increase

in $|H_x|$ is shown in the results of models 1 and 3. The larger gradients in $|H_x|$ near the coastline for the higher frequencies are a result of the skin effect.

In both models 1 and 3, it is evident from examination of Fig. 7 that the proportionate increase in H_z at the coastline is much greater than the proportionate increase in H_x. Also, the profiles of $|H_z/H_x|$ show a greater frequency dependence for model 1 than for model 3.

From Fig. 7 it is seen that $|E_y/H_x|$ profiles at a given frequency show the expected increase in this ratio in going from the sea to the continent. For all models, the $|E_y/H_x|$ curve has a steeper slope near the coastline at 0.3 hz than at 0.03 hz.

At low frequencies, the mantle structure has a greater effect on the surface ocean currents than at high frequencies. This is shown in the behaviour of $|E_y|$ over the ocean in Figs. 5 and 6. At a frequency of 0.3 hz, the $|E_y|$ values for models 1 and 3 are very similar. At 0.03 hz, the oceanic $|E_y|$ values for model 3 are less than those of model 1. This is expected, since at low frequencies currents are more intense in the mantle and oceanic currents are reduced. Cox et al. (1970) claim that by knowing the magnitude of surface electric currents in the ocean, the effect of the mantle on the coastal magnetic variations may be estimated.

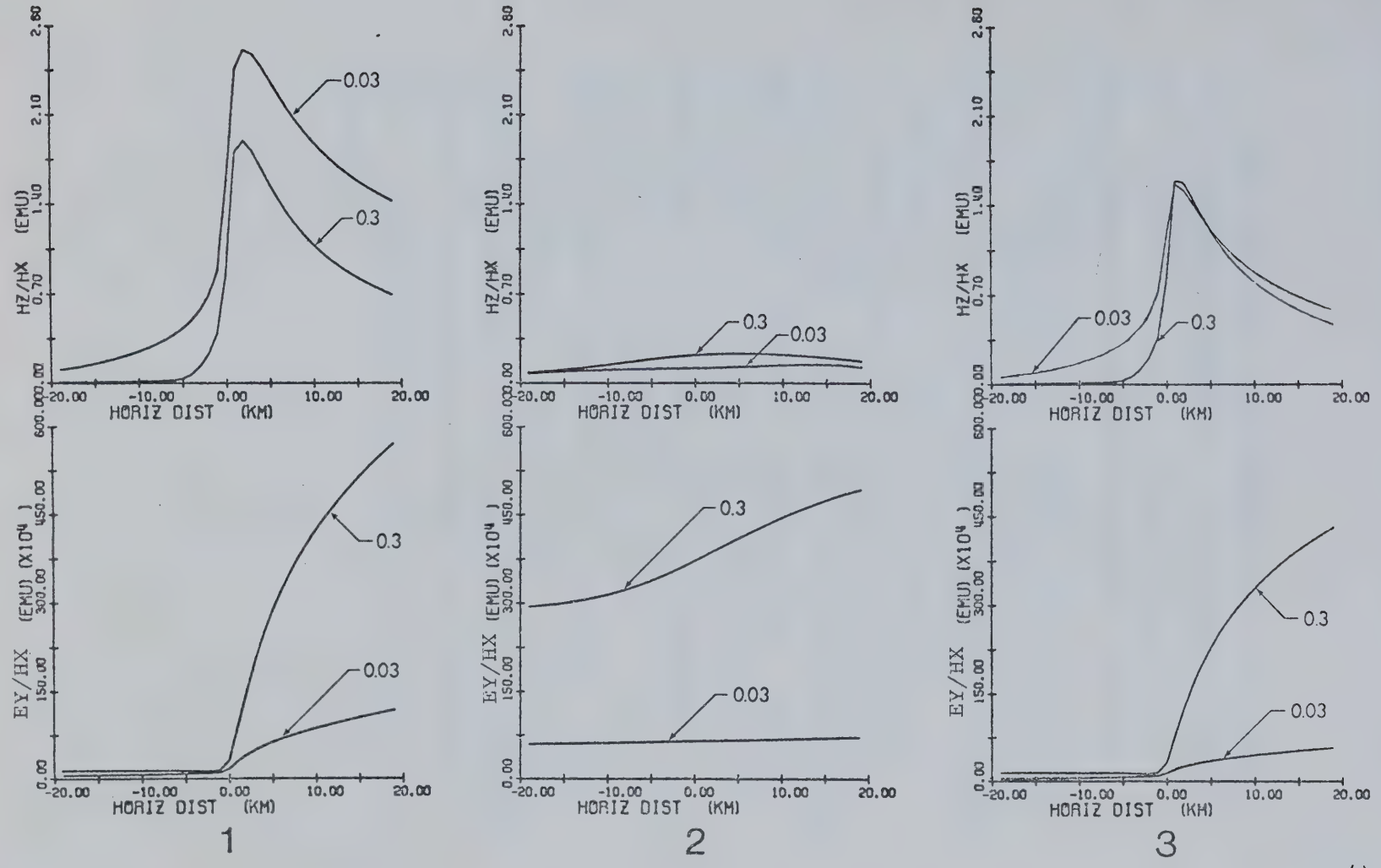

Fig. 7. Profiles of $|E_y/H_x|$ and $|H_z/H_x|$ for the three two-dimensional models.

(Number under each set of graphs corresponds to the model number.)

The behaviour of the phases of E_y, H_x, and H_z is also frequency dependent. In both models 1 and 3, the changes in the phases are more abrupt at the higher frequency due to the skin effect. For the high frequency profiles of models 1 and 3, minimum values in the phases of E_y, H_x, and H_z occur near the coastline. At the lower frequency of 0.03 hz, changes in the phase for all models are gradual.

From comparisons of the results for all three models considered, it is evident that the electric and magnetic fields shown for model 3 are not a simple superposition of the fields for models 1 and 2. The fields appear to be caused by an electromagnetic coupling between the conducting structures of the crust, ocean, and mantle, as pointed out by Rikitake (1966).

The similarity in the behaviour of the $\underline{E}$ and $\underline{H}$ components for models 1 and 3 emphasizes the difficulty involved in discriminating between the ocean effect, and the combined geomagnetic effect of the ocean and the mantle.

CHAPTER 3

A THREE-DIMENSIONAL NUMERICAL TECHNIQUE

3.1 General

Although the effect of some conductivity inhomogeneities on the earth's magnetic variation field may be studied by two-dimensional methods, there are many anomalies which must be analysed by three-dimensional methods. Treumann (1970) indicates that the Alert, Tucson and Japanese anomalies are examples of geomagnetic anomalies which are distinctly three-dimensional in nature. Treumann also suggests how a solution to the three dimensional problem may be obtained by use of the Green's tensor.

Recently, large arrays of magnetic instruments, as used by Gough and Reitzel (1969), Porath and Gough (1971), Camfield et al. (1971), and Camfield and Gough (1972) for magnetic depth sounding studies, have simultaneously measured the magnetic field components at many locations over considerable areas of the earth's surface. This led to the consideration of the induction problem in three dimensions by Jones and Pascoe (1972) who presented preliminary results for an imbedded cube.

Jones and Pascoe (1972) solved Maxwell's equations over a three-dimensional grid by use of finite difference

approximations and the Gauss-Seidel iterative method. The spacing of points in the grid was uniform, and the conductivity contrast in the models studied was small.

However, in modeling three-dimensional structures such as an island imbedded in an ocean, conductivity contrasts are great. In the island problem, the conductivity ratio between the ocean and the crust is about 4000. Furthermore, the vertical dimensions of the sea are small compared with the skin depths of the crust for the periods we are interested in. Therefore, the dimensions of the sea are small compared with the distances from lateral conductivity discontinuities to the boundaries which are necessary to accommodate the boundary conditions on the sides and bottom of the grid. (Refer to Pascoe and Jones, 1972 for a discussion of the boundary locations relative to lateral discontinuities for the two-dimensional case.)

For the island problem, it is necessary to provide for a large number of grid points within a uniform grid, or alternatively to provide for a grid which can be varied in size throughout the whole region so that large distances from the island may be accommodated in the model. (This condition is essential if the problem is to be a perturbation problem.) Since computation time increases considerably as the number of grid

points is increased, it is necessary to use a variable grid rather than a large grid of uniform spacing. Lines and Jones (1972a) have considerably extended the method of Jones and Pascoe (1972) so that a grid of variable dimensions may be used, and the basic method is discussed in the following section.

3.2 The Method of Solution

In the previous discussion of Maxwell's equations (section 1.2), the equation in $\underline{E}$

$$\nabla^2\underline{E} - \nabla(\nabla.\underline{E}) = i\eta^2\underline{E} \qquad (3.1)$$

(where $\eta^2 = 4\pi\sigma\omega$) was obtained. In the three-dimensional problem all components of $\underline{E}$ vary with x, y, and z in Cartesian coordinates.

The above vector equation in $\underline{E}$ may be rewritten as three scalar equations in Cartesian coordinates:

$$\frac{\partial^2 E_x}{\partial y^2} + \frac{\partial^2 E_x}{\partial z^2} - \frac{\partial}{\partial x}\left(\frac{\partial E_y}{\partial y} + \frac{\partial E_z}{\partial z}\right) = i\eta^2 E_x \ , \qquad (3.2)$$

$$\frac{\partial^2 E_y}{\partial x^2} + \frac{\partial^2 E_y}{\partial z^2} - \frac{\partial}{\partial y}\left(\frac{\partial E_x}{\partial x} + \frac{\partial E_z}{\partial z}\right) = i\eta^2 E_y \ , \qquad (3.3)$$

$$\frac{\partial^2 E_z}{\partial x^2} + \frac{\partial^2 E_z}{\partial y^2} - \frac{\partial}{\partial z}\left(\frac{\partial E_x}{\partial x} + \frac{\partial E_y}{\partial y}\right) = i\eta^2 E_z \ . \qquad (3.4)$$

These three equations are solved simultaneously for E_x, E_y, and E_z by the finite difference method.

In describing this numerical method, only equation (3.2) will be considered. However, a similar procedure is used in evaluating equations (3.3) and (3.4). An outline of the three-dimensional grid is shown in Fig. 8. The numerical formulation of the equations for a particular point '0' is considered. In general, distances to adjacent points in the grid are not equal, and eight conductivity regions surround the point '0'. The subscript on electric field components refers to the point on the grid of Fig. 8 at which the components are evaluated.

In equation (3.2), the finite difference expressions for $\partial^2 E_x/\partial y^2$ and $\partial^2 E_x/\partial z^2$ at the point '0' are evaluated by using the first three terms of a Taylor series expansion. Consider the evaluation of $\partial^2 E_x/\partial y^2$ at the point '0'. We may write:

$$E_{x3} = E_{xo} + \left(\frac{E_{x3} - E_{x4}}{d_3 + d_4}\right) d_3 + \frac{1}{2}\left(\frac{\partial^2 E_x}{\partial y^2}\right)_o d_3^2 \qquad (3.5)$$

and

$$E_{x4} = E_{xo} - \left(\frac{E_{x3} - E_{x4}}{d_3 + d_4}\right) d_4 + \frac{1}{2}\left(\frac{\partial^2 E_x}{\partial y^2}\right) d_4^2 \quad , \qquad (3.6)$$

where in these expressions central difference formulae have been used for $(\partial E_x/\partial y)_o$. The value of $(\partial^2 E_x/\partial y^2)_o$ is derived by combining (3.5) and (3.6):

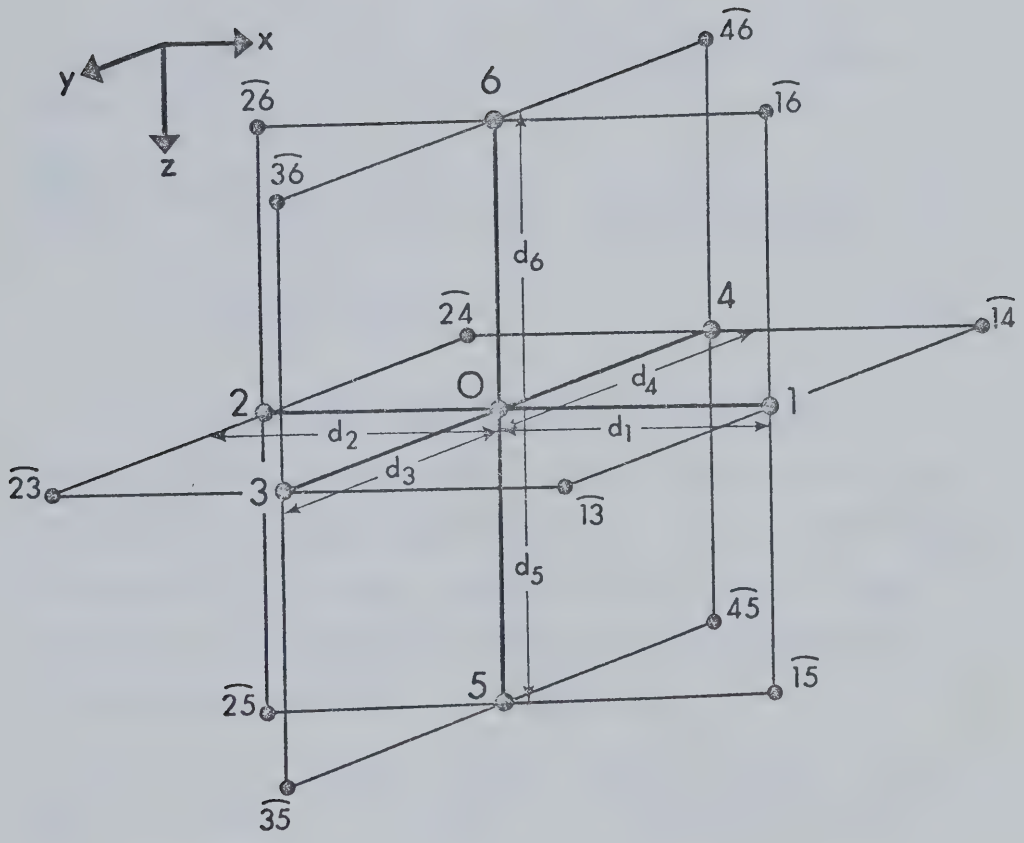

Fig. 8. An outline of the three-dimensional grid used.

$$\left(\frac{\partial^2 E_x}{\partial y^2}\right)_o = E_{x3}\left(\frac{1}{d_3^2} + \frac{1}{d_3+d_4}\left(\frac{1}{d_4} - \frac{1}{d_3}\right)\right) + E_{x4}\left(\frac{1}{d_4^2} + \frac{1}{d_3+d_4}\left(\frac{1}{d_3} - \frac{1}{d_4}\right)\right)$$

$$- E_{xo}\left(\frac{1}{d_3^2} + \frac{1}{d_4^2}\right) \quad . \tag{3.7}$$

The value of $(\partial^2 E_x/\partial z^2)_o$ is found in a similar manner:

$$\left(\frac{\partial^2 E_x}{\partial z^2}\right)_o = E_{x5}\left(\frac{1}{d_5^2} + \frac{1}{d_5+d_6}\left(\frac{1}{d_6} - \frac{1}{d_5}\right)\right) + E_{x6}\left(\frac{1}{d_6^2} + \frac{1}{d_5+d_6}\left(\frac{1}{d_5} - \frac{1}{d_6}\right)\right)$$

$$- E_{xo}\left(\frac{1}{d_5^2} + \frac{1}{d_6^2}\right) \quad . \tag{3.8}$$

To evaluate the mixed partial derivatives, $\partial/\partial x(\partial E_y/\partial y)$ and $\partial/\partial x(\partial E_z/\partial z)$, we again rely on the use of central difference approximations. To find $\partial/\partial x(\partial E_y/\partial y)$ at the point '0', we use central differences, in the x direction, of the central difference expressions for $\partial E_y/\partial y$ nearest the point '0'. That is,

$$\frac{\partial}{\partial x}\left(\frac{\partial E_y}{\partial y}\right)_o = \frac{1}{d_1+d_2}\left\{\frac{(E_{y\widehat{13}} - E_{y\widehat{14}})}{d_3+d_4} - \frac{(E_{y\widehat{23}} - E_{y\widehat{24}})}{d_3+d_4}\right\} \tag{3.9}$$

and

$$\frac{\partial}{\partial x}\left(\frac{\partial E_z}{\partial z}\right)_o = \frac{1}{d_1+d_2}\left\{\frac{(E_{z\widehat{15}} - E_{z\widehat{16}})}{d_5+d_6} - \frac{(E_{z\widehat{25}} - E_{z\widehat{26}})}{d_5+d_6}\right\} . \tag{3.10}$$

Upon substitution of the expressions for $(\partial^2 E_x/\partial y^2)_o$, $(\partial^2 E_x/\partial z^2)_o$, $\partial/\partial x(\partial E_y/\partial y)_o$, and $\partial/\partial x(\partial E_z/\partial z)_o$ into equation (3.2), we obtain a finite difference expression given

by

$$-E_{xo}\left(\frac{1}{d_3^2}+\frac{1}{d_4^2}+\frac{1}{d_5^2}+\frac{1}{d_6^2}\right) + E_{x3}D_3 + E_{x4}D_4 + E_{x5}D_5 + E_{x6}D_6$$

$$- \frac{1}{d_1+d_2}\left\{\frac{1}{d_3+d_4}\left(E_{y\widehat{13}} - E_{y\widehat{14}} - E_{y\widehat{23}} + E_{y\widehat{24}}\right)\right.$$

$$\left. + \frac{1}{d_5+d_6}\left(E_{z\widehat{15}} - E_{z\widehat{16}} - E_{z\widehat{25}} + E_{z\widehat{26}}\right)\right\} = i\eta^2 E_{xo} \qquad (3.11)$$

where

$$D_3 = \frac{1}{d_3^2} + \frac{1}{d_3+d_4}\left(\frac{1}{d_4} - \frac{1}{d_3}\right)$$

$$D_4 = \frac{1}{d_4^2} + \frac{1}{d_3+d_4}\left(\frac{1}{d_3} - \frac{1}{d_4}\right)$$

$$D_5 = \frac{1}{d_5^2} + \frac{1}{d_5+d_6}\left(\frac{1}{d_6} - \frac{1}{d_5}\right)$$

and

$$D_6 = \frac{1}{d_6^2} + \frac{1}{d_5+d_6}\left(\frac{1}{d_5} - \frac{1}{d_6}\right) \quad .$$

This equation and similar representations for equations (3.3) and (3.4) must be simultaneously satisfied at each interior point of each region.

The finite difference representations for (3.3) and (3.4) are:

$$-E_{yo}\left(\frac{1}{d_1^2}+\frac{1}{d_2^2}+\frac{1}{d_5^2}+\frac{1}{d_6^2}\right) + E_{y1}D_1 + E_{y2}D_2 + E_{y5}D_5 + E_{y6}D_6$$

$$- \frac{1}{d_3+d_4}\left\{\frac{1}{d_1+d_2}\left(E_{x\hat{13}} - E_{x\hat{23}} - E_{x\hat{14}} + E_{x\hat{24}}\right)\right.$$

$$\left. + \frac{1}{d_5+d_6}\left(E_{z\hat{35}} - E_{z\hat{36}} - E_{z\hat{45}} + E_{z\hat{46}}\right)\right\} = i\eta^2 E_{yo} \qquad (3.12)$$

and

$$-E_{zo}\left(\frac{1}{d_1^2}+\frac{1}{d_2^2}+\frac{1}{d_3^2}+\frac{1}{d_4^2}\right) + E_{z1}D_1 + E_{z2}D_2 + E_{z3}D_3 + E_{z4}D_4$$

$$- \frac{1}{d_5+d_6}\left\{\frac{1}{d_1+d_2}\left(E_{x\hat{15}} - E_{x\hat{25}} - E_{x\hat{16}} + E_{x\hat{26}}\right)\right.$$

$$\left. + \frac{1}{d_3+d_4}\left(E_{y\hat{35}} - E_{y\hat{45}} - E_{y\hat{36}} + E_{y\hat{46}}\right)\right\} = i\eta^2 E_{zo} \qquad (3.13)$$

where

$$D_1 = \frac{1}{d_1^2} + \frac{1}{d_1+d_2}\left(\frac{1}{d_2} - \frac{1}{d_1}\right)$$

and

$$D_2 = \frac{1}{d_2^2} + \frac{1}{d_1+d_2}\left(\frac{1}{d_1} - \frac{1}{d_2}\right) \quad .$$

As in the two-dimensional work of Jones and Pascoe (1971), these equations are written for each conductive region surrounding the point '0'. The 'fictitious' values (Smith (1969), Jones and Pascoe (1971)) must be eliminated by application of the internal boundary conditions. Application of the boundary condition that tangential components

of $\underline{E}$ and $\underline{H}$ must be continuous eliminates 2/3 of the 'fictitious' values. However, a problem arises when $\underline{E}$ is normal to a boundary for which σ is discontinuous. We know that the normal component of $\underline{J}$ $(=\sigma\underline{E})$ must be continuous across a boundary. If σ is discontinuous at a boundary, the normal component of $\underline{E}$ is also discontinuous. A discontinuity in $\underline{E}$ at a boundary cannot be represented by a point value at the boundary. This is an inherent property of a pointwise solution to the problem. Therefore, the average of the values of $\underline{E}$ on each side of the boundary is actually used. When expressions (3.11), (3.12) and (3.13) are summed over all eight regions surrounding the point '0' and boundary conditions are applied to $\underline{E}$, the resulting expressions are of the same form as in (3.11), (3.12) and (3.13) with η^2 being replaced by $\overline{\eta^2}$, where $\overline{\eta^2}$ is the average of η^2 for all regions surrounding the point '0'.

These resulting finite difference equations are solved simultaneously for E_x, E_y, and E_z by use of the Gauss-Seidel method. The Gauss-Seidel numerical method is a standard relaxation technique for solving simultaneous linear equations. In this method, the values of E_x, E_y and E_z for a given point are calculated in terms of the values of E_x, E_y and E_z for surrounding points by use of the finite difference equations. These calculated values are then used immediately in the iterative process

to determine values of $\underline{E}$ at other points in the grid. In each iteration, the values of E_x, E_y and E_z are calculated throughout the grid in terms of the values of the surrounding points. (Only the values of $\underline{E}$ at the outermost points of the grid remain fixed).

Initially, values are required throughout the grid to start the iterative process. These initial values can be determined for certain structures of a one-dimensional or two-dimensional nature. Determination of the initial values may be done analytically, as in the case of a layered half-space, or numerically, as in the case of a two-dimensional coastline structure.

In using the variable grid of Fig. 8, it is advantageous to make the grid intervals small and uniform in regions near the conductivity inhomogeneities where the electromagnetic fields are expected to vary most rapidly. By designing the grid in this manner, the central difference formulae are a better approximation to the derivatives of the field components. Farther from the three-dimensional inhomogeneities, the grid intervals can be increased in size so as to accommodate the external boundary values.

After each iteration, a residual term is calculated. This residual is taken as the maximum value for the difference between values of E_x, E_y and E_z from the

particular iteration being considered and the values of E_x, E_y and E_z from the previous iteration for all points in the grid. The iteration process continues until the calculated residual is less than a specified value. All models calculated have exhibited convergence.

After a solution has been obtained for $\underline{E}$, the values of $\underline{H}$ are determined from the equation

$$\underline{H} = - \frac{1}{i\omega} (\nabla \times \underline{E}) \ . \qquad (3.14)$$

The curl of $\underline{E}$ is determined by use of central difference formulae.

CHAPTER 4

RESULTS FROM THE THREE-DIMENSIONAL METHOD

4.1 Investigation of the "Island Effect"

During recent years, much attention has been paid to studies of the "island effect". Recent investigations include those of Mason (1963), Edwards et al. (1971), and Klein (1971). The island effect refers to the geomagnetic effects caused by the interruption of electric current flow in the oceans by island structures. Price (1967) points out that the induced system will usually be of large dimensions compared with the size of the island. The island perturbs the current system so that currents divide and stream past the island structure. The flow of electric currents around the islands, which largely determines the magnetic field near the edges of the islands, can cause the vertical component of the magnetic field to be in opposite directions on opposite sides of the island (Price, 1967).

4.1.1 Description of Models

Three-dimensional inhomogeneities in a layered half-space represent the island structures. To investigate the "island effect", the layered half-space consists of an upper layer to represent an ocean of depth 2 km overlying a more

resistive layer which represents the crust. The island structures are of the same conductivity as the crust, and protrude up from the underlying crustal material to the surface of the conducting half-space. Two different structures are studied for sinusoidally time-varying source fields of three different frequencies and these are shown in Fig. 9. Model (a) is a single island, and model (b) has two islands. All islands have a shelf structure. A uniform source with sinusoidal time variation ($E_x = E_o e^{i\omega t}$, $E_y = E_z = 0$) is assumed over the uppermost boundary plane of the grid (which for this model was taken 57 km above the surface). The conductivities are given in Table 3 for the ocean and the crust along with the skin depths for the frequencies used. The grid is variable, and identical for both models. The four vertical planes which constitute the sides of the grid are taken to be sufficiently far from the island structures so that a two-layered uniformly stratified subsurface may be assumed at the boundaries. The dimensions of the grid, which consists of a $23 \times 23 \times 23$ array of points, are given in Table 4. The islands are located within the uniform grid region in the x-y plane as illustrated in Fig. 10. Results presented in the following section illustrate contours and profiles of the amplitudes within the uniform grid region surrounding the islands.

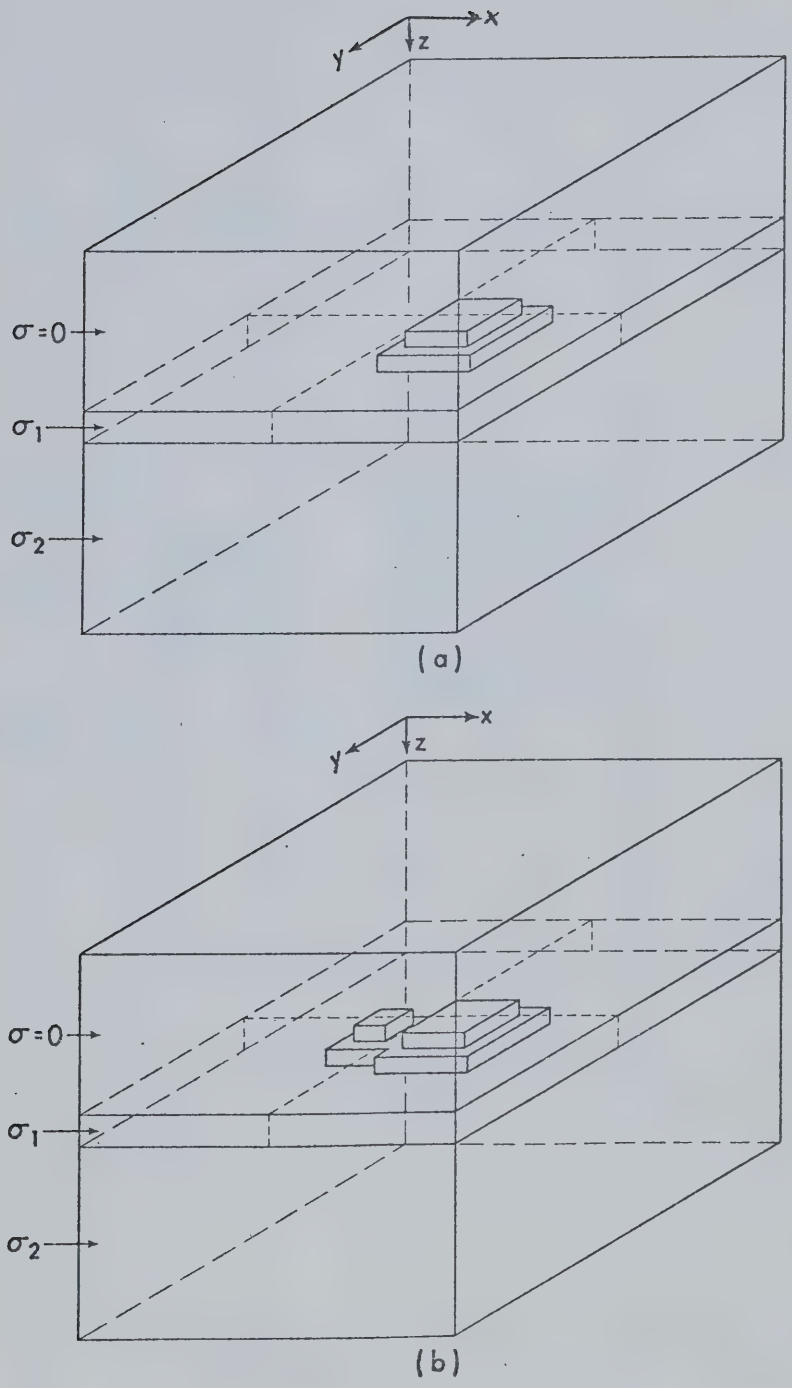

Fig. 9. The three-dimensional island structures:
a) Single island structure
b) Two-island structure

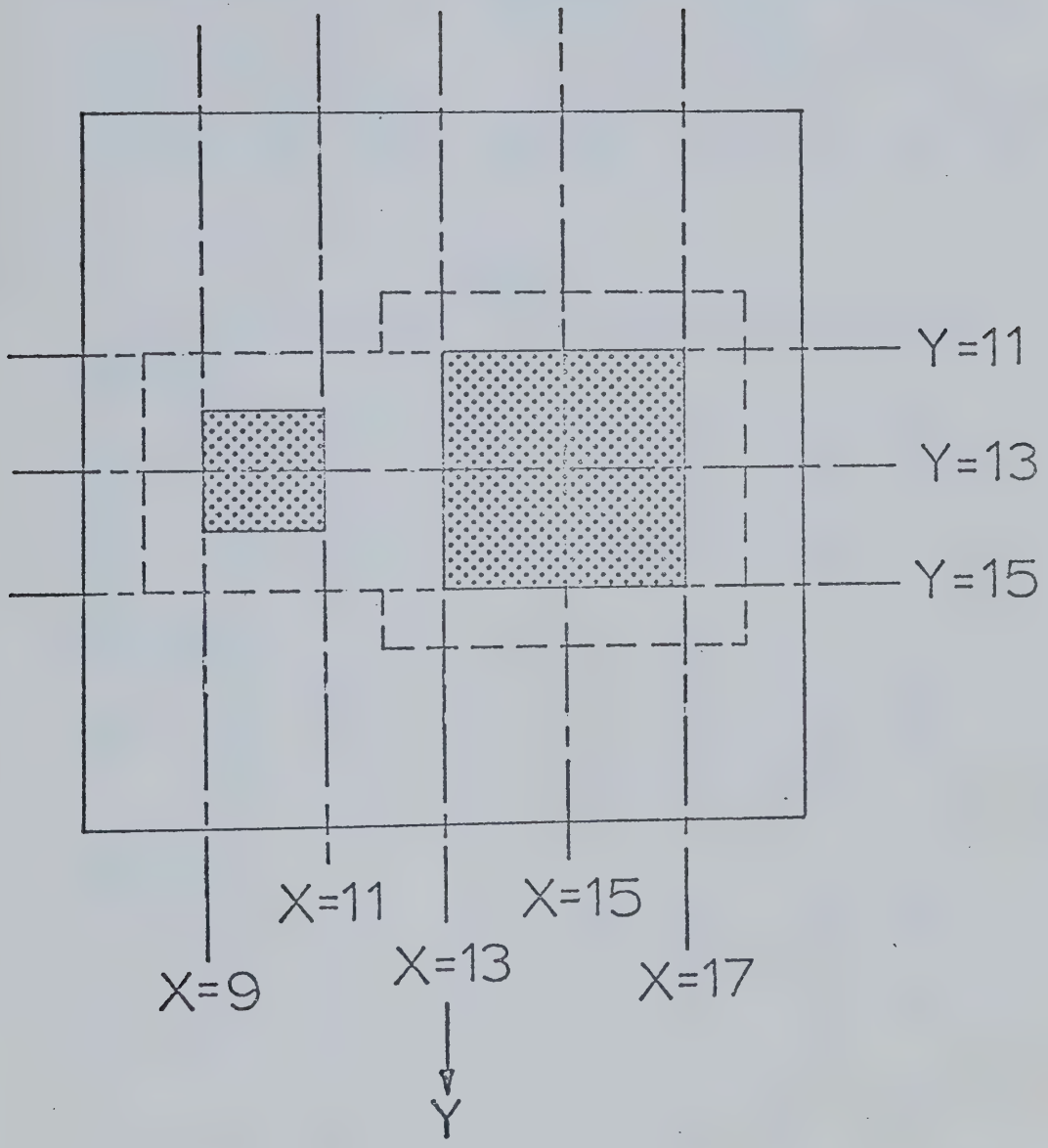

Fig. 10. The uniform grid region surrounding the islands with some of the profiles considered.

Table 3

Conductivities and skin depths for the island models

Conductivites	Skin depths at different periods		
	1 min.	10 min.	30 min.
$\sigma = 0$ (air)	----------	infinite	----------
$\sigma_1 = 4\times10^{-11}$ emu (ocean)	1.95 km	6.15 km	10.68 km
$\sigma_2 = 1\times10^{-14}$ emu (crust)	123.28 km	389.84 km	675.22 km

Table 4

Grid spacing for the island models (in kilometers)

X direction

	45.00	15.00	5.00	3.00	2.00	1.00	1.00
1.00	1.00	1.00	1.00	1.00	1.00	1.00	1.00
1.00	1.00	2.00	3.00	5.00	15.00	45.00	

Y direction

	45.00	15.00	5.00	3.00	2.00	1.00	1.00
1.00	1.00	1.00	1.00	1.00	1.00	1.00	1.00
1.00	1.00	2.00	3.00	5.00	15.00	45.00	

Z direction

18.00	12.00	9.00	7.00	5.00	3.00	2.00
1.00 | 1.00	1.00	1.00	1.00	2.00	3.00	
10.00	20.00	40.00	80.00	90.00	90.00	90.00

(The vertical line denotes the position of the surface plane.)

The sinusoidally time-varying source has periods of one, ten, and thirty minutes. Results for the two different structures are given for all three source periods. The value of $|E_x|$ is normalized to 1.0 at the surface for the outer boundaries of the grid.

4.1.2 Results and Discussion

The effect on the phases and amplitudes of the $\underline{E}$ and $\underline{H}$ components due to the single island structure is compared with the effect of the two island structure for the three different source periods in Figs. 11, 12 and 14-27. From these figures it is seen that the presence of the smaller island in the two-island model considerably modifies the $\underline{E}$ and $\underline{H}$ fields near the larger island.

At the surface of the conducting region, the effects on the amplitude contours and profiles of the $\underline{E}$ and $\underline{H}$ components, due to the two different structures are compared in Figs. 11, 12 and 14 to 21. Contours are drawn over the uniform grid region shown in Fig. 10. Within this region the grid dimensions are one kilometer. Profiles in the x and y directions are drawn and are referenced by the row or column of the surface grid shown in Fig. 10. From the profile values, the values of the contours in the contour plots may be determined.

4.1.2.1 Amplitudes for a Source of One Minute Period

Contours of the amplitude of E_x for the single island and a source period of one minute are given in Fig. 11. For these contours, a maximum in $|E_x|$ occurs at the center of the island. For the case of two islands, an additional maximum in $|E_x|$ is evident at the position of the smaller island. The difference in $|E_x|$ for the two structures is demonstrated by a comparison of the amplitude profiles of E_x for the profiles Y = 13 shown in Figs. 18 and 19. Along these 12 km profiles, the point y = 0.0 km, x = 0.0 km is the center of the uniform grid region of Fig. 10.

For the single island structure, contours of $|E_y|$ are symmetrical about the center of the island. With the two island structure, it is noted that the two maxima of $|E_y|$ on the left hand side of the contoured area are at different positions from those of the single island $|E_y|$ contours, due to the effect of the smaller island.

The behaviour of the amplitude of E_y agrees with the physical interpretation concerning electric field line flow around an insulator. A diagram illustrating such flow in the oceans in the x-y and x-z planes is shown in Figs. 13(a) and 13(b). As is evident from the calculations, this figure illustrates that the maxima of $|E_y|$ appear at the corners of the islands due to the bending

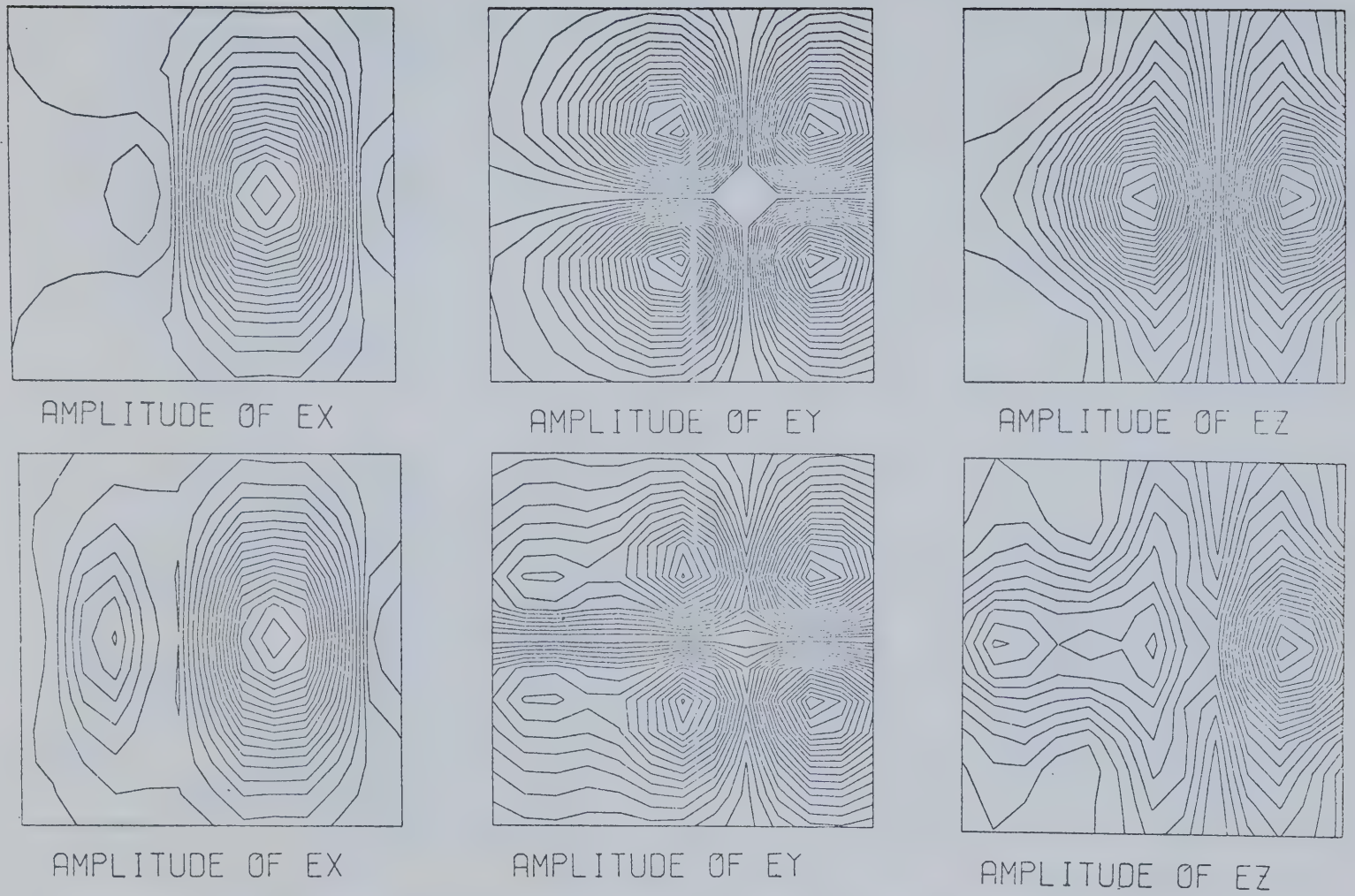

Fig. 11. Amplitude contours of E_x, E_y and E_z for a source period of one minute. Top: single island structure. Bottom: two-island structure.

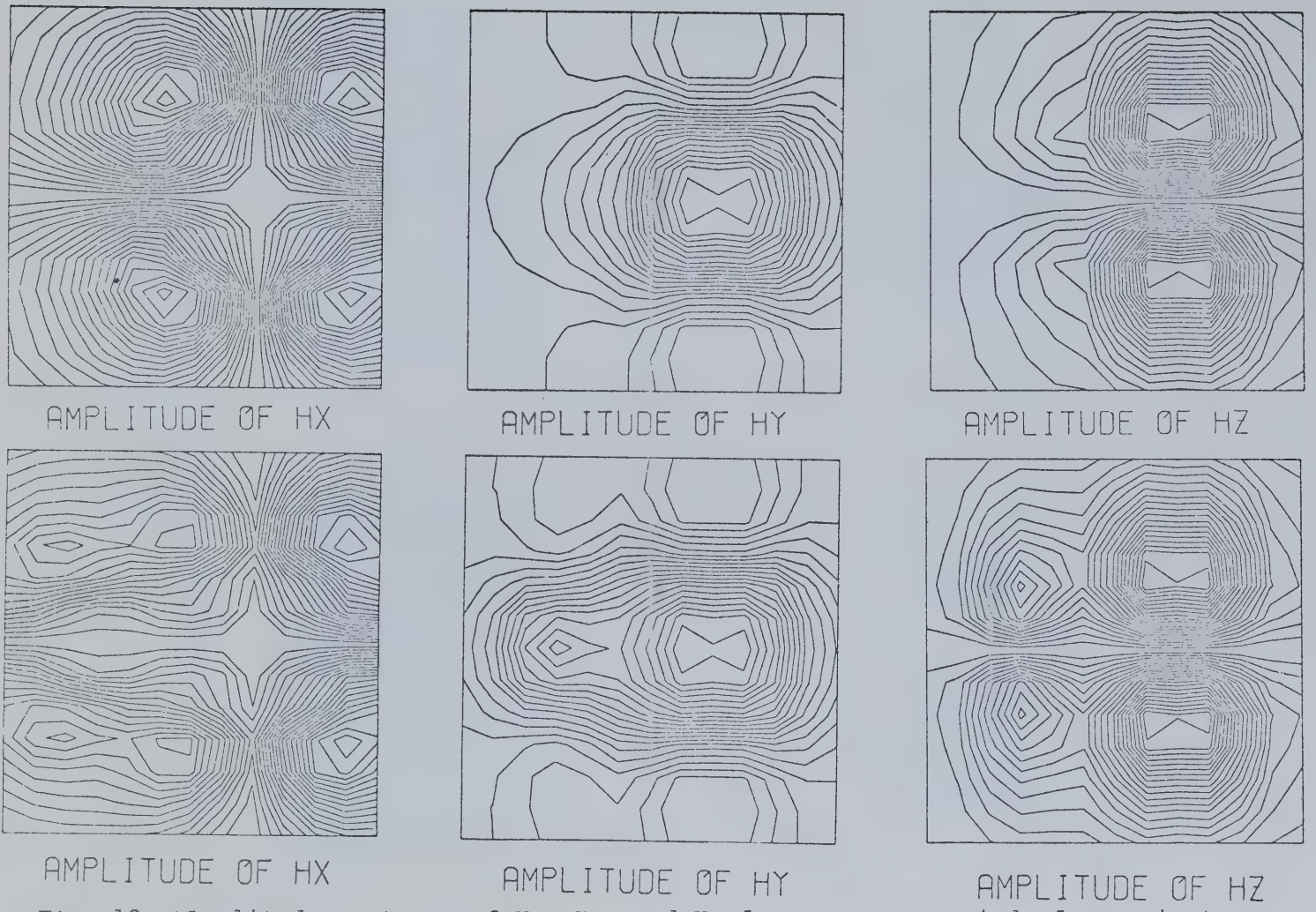

Fig. 12. Amplitude contours of H_x, H_y, and H_z for a source period of one minute. Top: single island structure. Bottom: two-island structure.

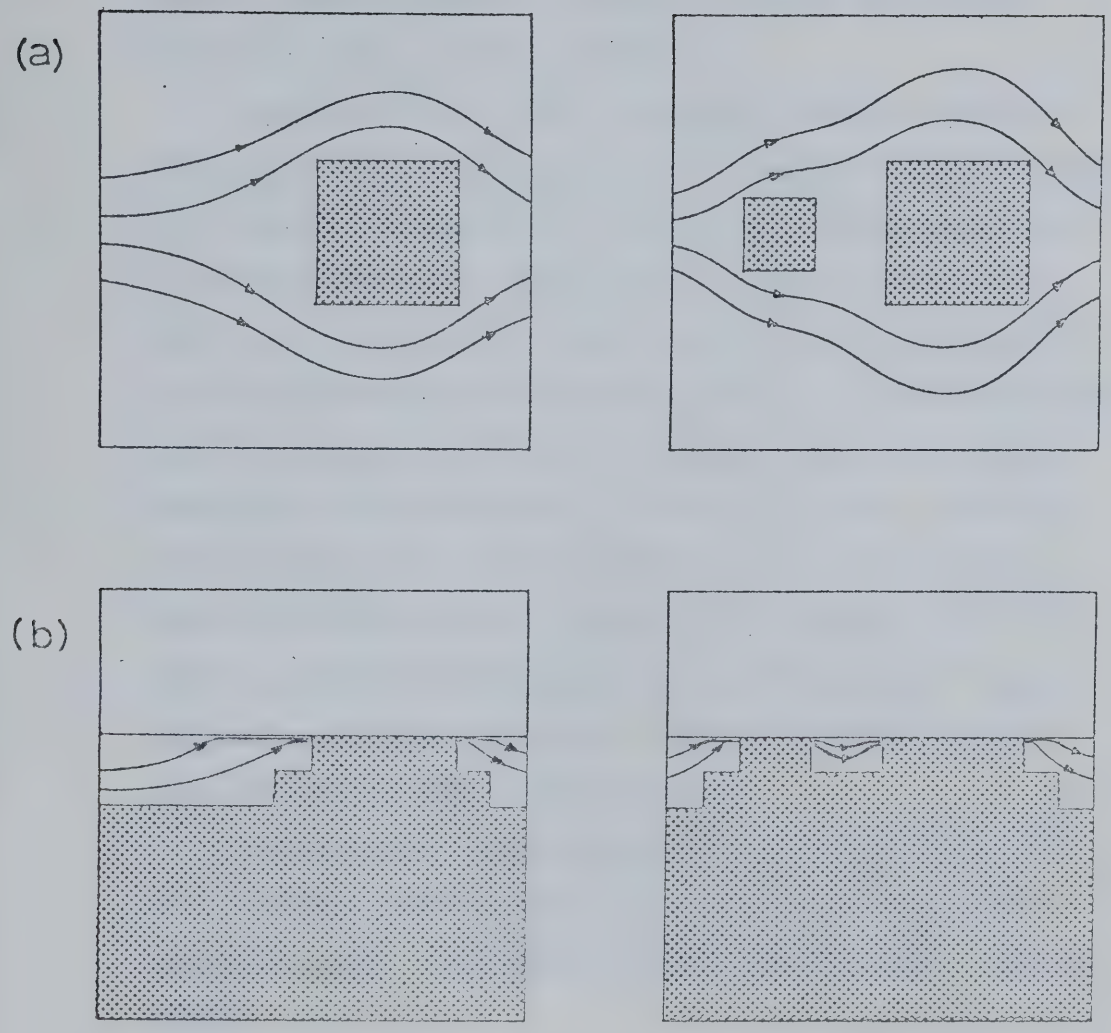

Fig. 13. Expected flow of electric current lines near the two structures considered.
a) Current flow in x-y plane
b) Current flow in x-z plane

of currents around the corners. The expected sign changes in E_y are also found in the calculated results and are demonstrated in the later section which discusses the phase of the $\underline{E}$ components.

Contours of $|E_z|$ for the single island in Fig. 11 show two maxima at the edge of the single islands centered about the Y = 13 profile. For the two-island structure, it is noted from the amplitude contours and profiles of Figs.11 and 19 that the local maxima in $|E_z|$ develop due to the presence of the smaller island. It should be noted that the amplitudes of E_z are largest where the vertical subsurface currents of Fig. 13(b) are largest. Although the behaviour of E_z is influenced by the averaging of conductivities on either side of the boundary, Price has given a physical explanation for the behaviour of E_z at the surface of the conductor, both in his 1967 review paper and by private communication.

Price (1967) shows that the charge on the surface of a conductor is non-zero and is given by the boundary condition on $\underline{D}$, the electric displacement vector. We can write

$$D_z' - D_z'' = -4\pi\beta \qquad (4.1)$$

or

$$\varepsilon' E_z' - \varepsilon'' E_z'' = -4\pi\beta \quad . \qquad (4.2)$$

In these equations, β is the surface charge density, the primed quantities refer to the medium just outside the

conductor, and the double primed quantities refer to the medium just inside the conductor.

By the equation of continuity,

$$J_z'' = -\frac{\partial \beta}{\partial t} \quad , \tag{4.3}$$

where J_z'' is the current density impinging on the surface from within the conducting ocean. But,

$$J_z'' = \sigma E_z'' = -\frac{\partial \beta}{\partial t} \quad , \tag{4.4}$$

so that in substituting in (4.4) for the value of E_z'' given in (4.2), we obtain

$$\frac{\varepsilon''}{\sigma}\frac{\partial \beta}{\partial t} + 4\pi\beta = -\varepsilon' E_z' \quad . \tag{4.5}$$

Since the time variation of the electric field is sinusoidal, the solution for β in (4.5) will also have a sinusoidal time variation, and $\partial\beta/\partial t = i\omega\beta$. Also, since by neglecting displacement currents we imply that $\omega << \sigma/\varepsilon''$, the first term of (4.5) is negligible in comparison with the second. Therefore, by (4.5) the minute charge distribution, β, is of order $-c^{-2}E_z'$. Also, from (4.4),

$$E_z'' = -\frac{1}{\sigma}\frac{\partial \beta}{\partial t} \quad , \tag{4.6}$$

and since we have shown that $\left|\frac{\varepsilon''}{\sigma}\frac{\partial \beta}{\partial t}\right| << |4\pi\beta|$, then

$$|E_z''| << \left|\frac{4\pi\beta}{\varepsilon''}\right| \quad . \tag{4.7}$$

That is,

$$|E_z''| << \left|\frac{\varepsilon'}{\varepsilon''} \; E_z'\right| \quad . \tag{4.8}$$

From (4.8), it is seen that the electric field just inside the conductor is generally negligible when compared with the electric field just outside the surface. Therefore, the same minute time-varying surface charge which causes a nonzero electric field (E_z') outside the conductor reduces the vertical component of the electric field just inside the conductor to a negligible value, so that currents inside the conductor flow parallel to the surface. Price emphasizes that the current required to set up the surface charge ($\sigma E_z''$) has a negligible magnetic effect.

The effect of a nonzero E_z' is shown in our results. Furthermore, since the size of the surface charge needed to cancel E_z just inside the surface of the conducting ocean depends on the strength of subsurface currents, the amplitude of E_x in our results is largest over regions where the vertical components of subsurface currents are largest. For all models, it should also be recognized that the amplitude of E_x is more than an order of magnitude greater than $|E_z|$.

Changes in the H_z component result from the perturbation of current flow in the x-y plane due to the

presence of the island structure. The island essentially creates a hole in the current flow pattern in the x-y plane, as shown in Fig. 13(a). Application of the right hand rule relating currents to magnetic fields gives a qualitative understanding of the behaviour of H_z. A comparison of the x-y current flow for the two different types of island structures (shown in Fig. 13(a)) explains the difference in the behaviour of $|H_z|$ for the two structures, as shown in Figs. 12, 20, and 21. Clearly, currents bending around the smaller island cause the additional maxima observed in the $|H_z|$ contours and profiles for the two island case.

The amplitude contours of the magnetic field components shown in Fig. 12 support the statement by Mason (1963) that the optimum position for making geomagnetic measurement on an island is near its center. Near the center, the "island effect" on the earth's magnetic variation field is minimized.

The amplitude of H_y is determined by current flow in the x-z plane. Since electric current flow is less inside the islands which act as insulators relative to the sea, minima in $|H_y|$ are observed over the islands. Figs. 12, 20, and 21 give the amplitude contours and profiles of $|H_y|$.

It is interesting to note that the amplitude contours of H_x display a similar behaviour to those of E_y.

The maxima of $|H_x|$ occur near the corners of the islands and are caused by the increased Y component of electric currents flowing around the poorly conducting crustal material of the islands.

The effect of the islands on the $\underline{E}$ and $\underline{H}$ components changes for different source periods.

4.1.2.2 Amplitudes for a Source of Ten Minute Period

For a ten minute source period, the amplitude contours and profiles of Figs. 14, 15 and Figs. 18-21 show a distinct difference in the $\underline{E}$ and $\underline{H}$ values for the single island structure as compared to the values for the two-island structure. These differences are basically due to the same effects as noticed in the previous case for a source period of one minute.

Skin effects are shown from the comparison of amplitude profiles for a source period of one minute with those for source periods of ten and thirty minutes. The skin depth, given by $(2\pi\sigma\omega)^{-\frac{1}{2}}$ in electromagnetic units, is a measure of field penetration into the conductor. At longer periods, the two-island structure appears as one large island due to the deeper penetration of the induced current system. The shallow features of the two-island system are more evident at shorter periods.

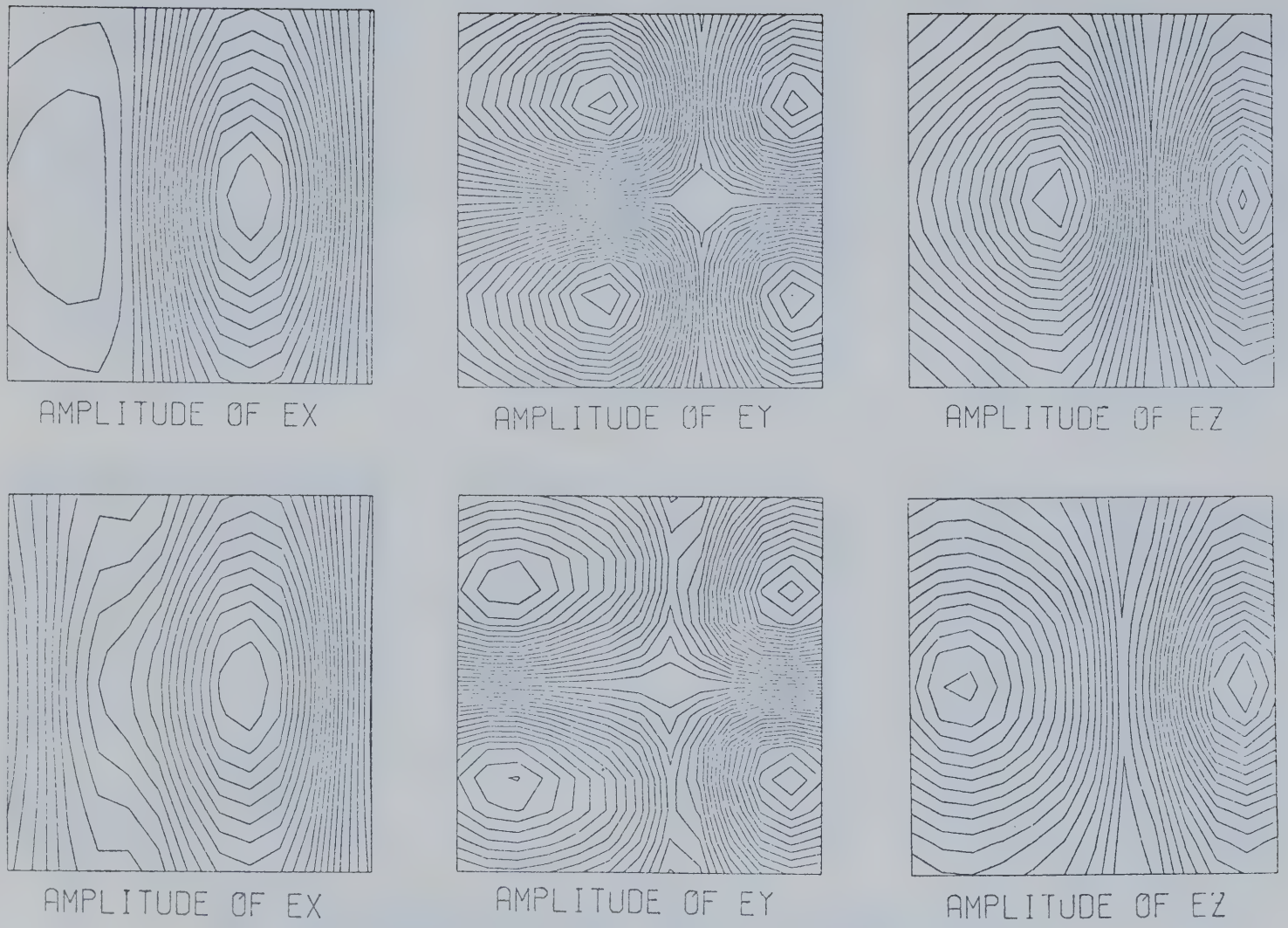

Fig. 14. Amplitude contours of E_x, E_y, and E_z for a source period of ten minutes. Top: single island structure. Bottom: two-island structure.

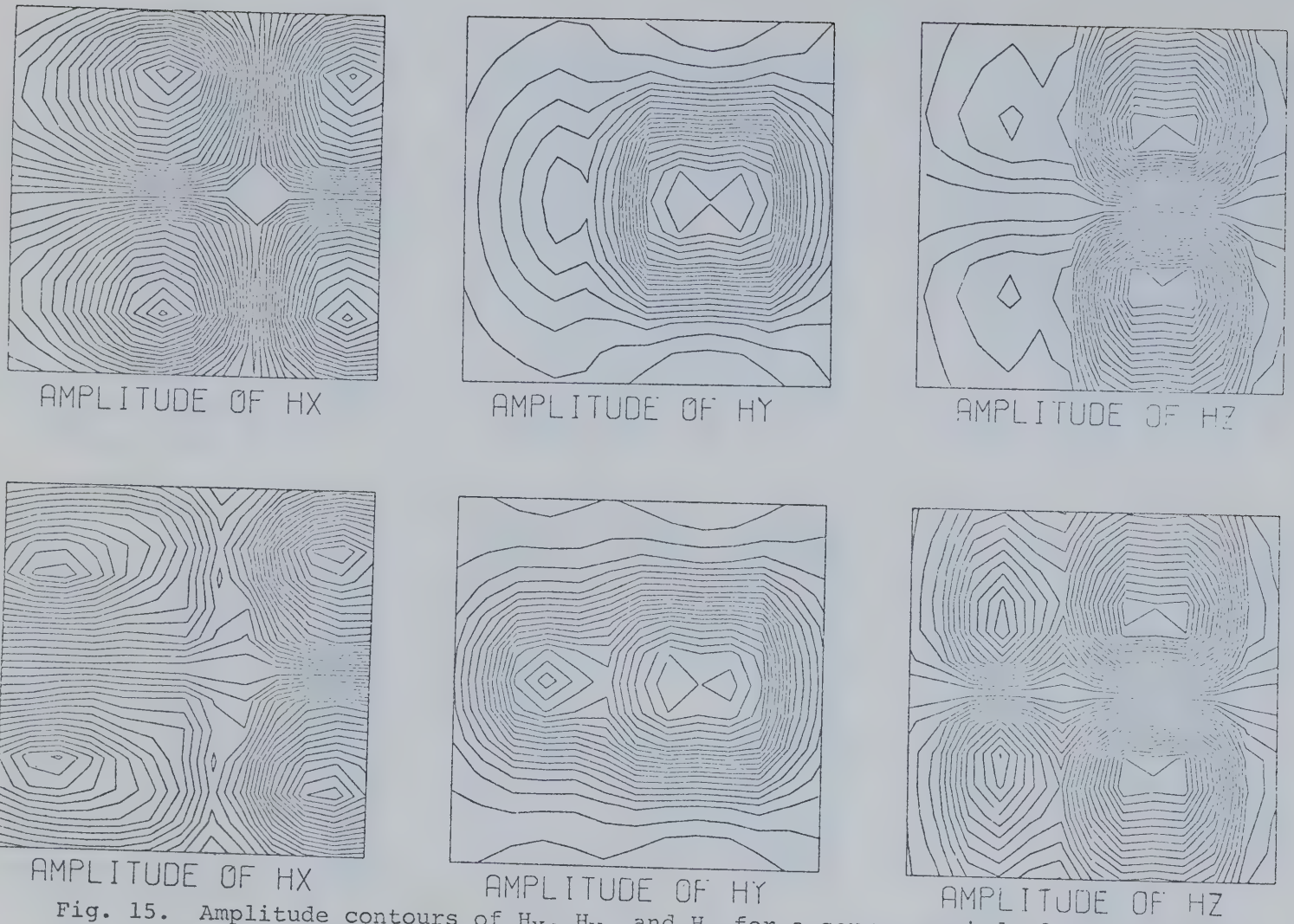

Fig. 15. Amplitude contours of H_x, H_y, and H_z for a source period of ten minutes. Top: single island structure. Bottom: two-island structure.

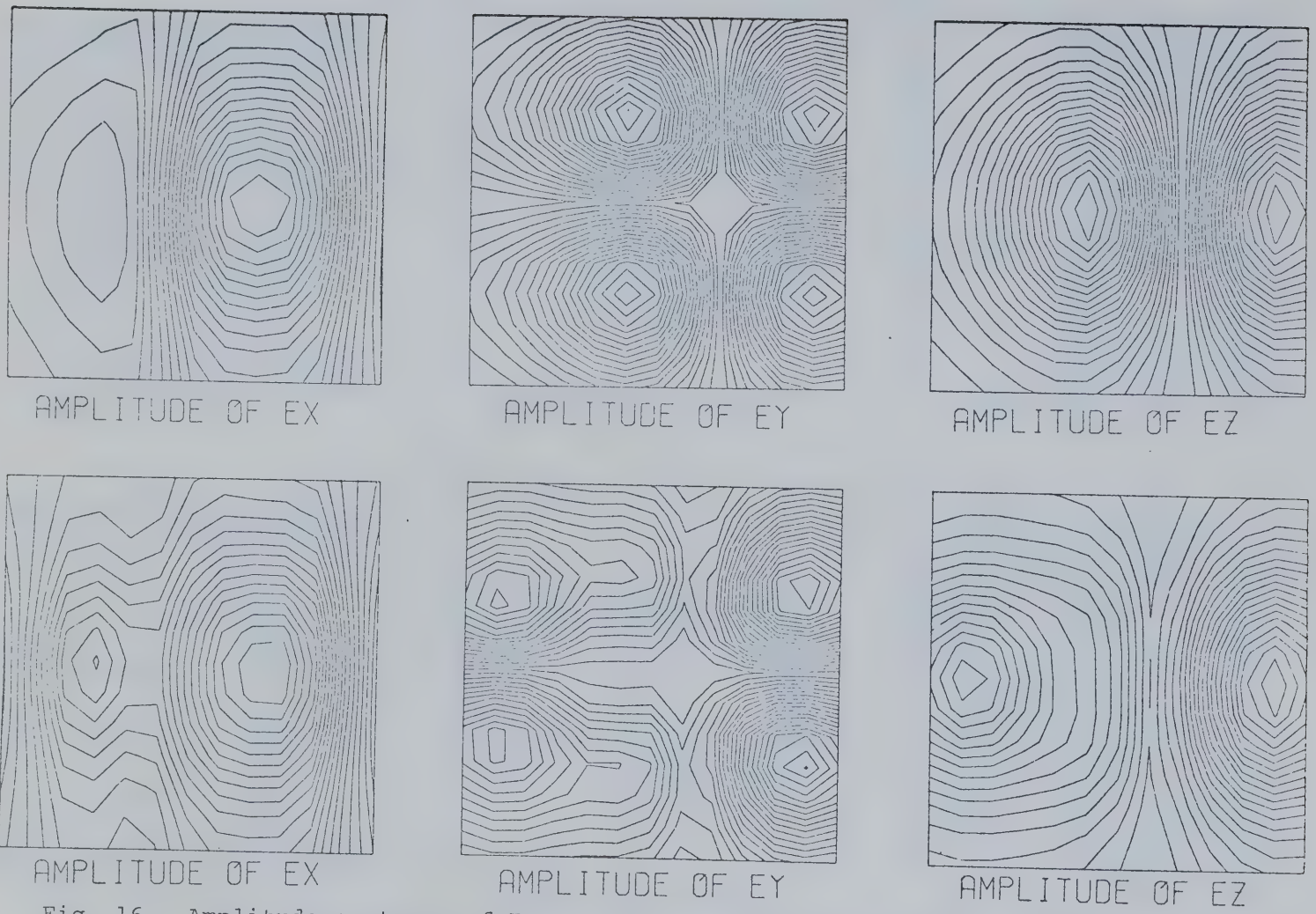

Fig. 16. Amplitude contours of E_x, E_y, and E_z for a source period of thirty minutes. Top: single island structure. Bottom: two-island structure.

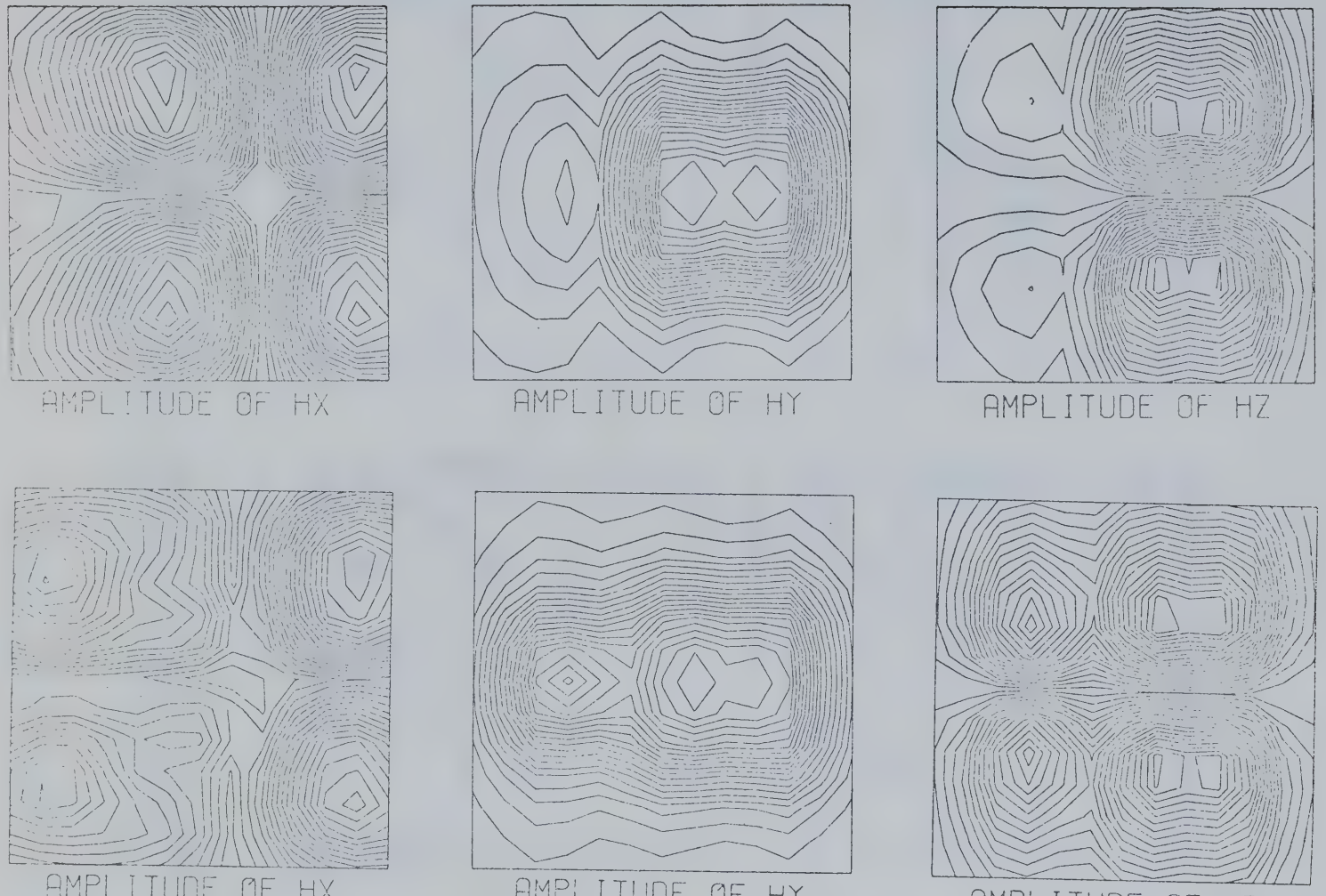

Fig. 17. Amplitude contours of H_x, H_y, and H_z for a source period of thirty minutes. Top: single island structure. Bottom: two-island structure.

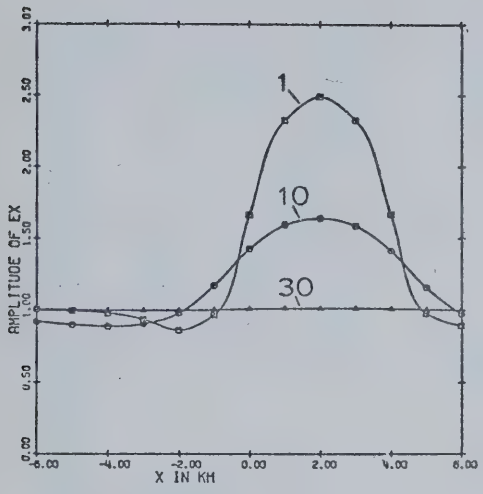

AMPLITUDE OF EX AT Y=13

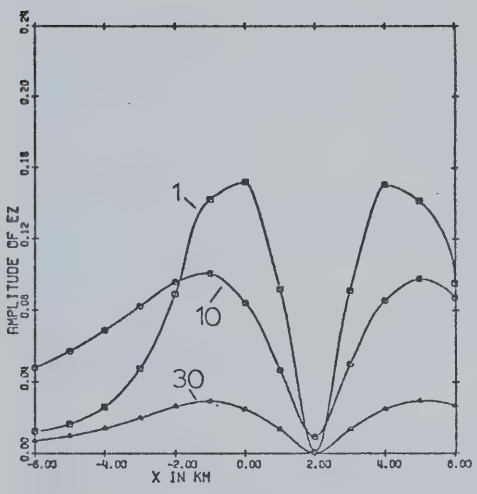

AMPLITUDE OF EZ AT Y=13

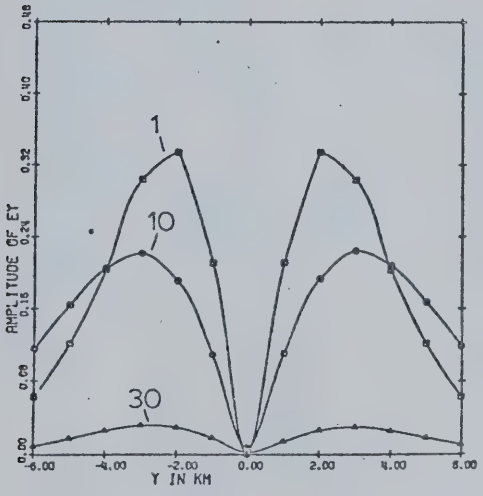

AMPLITUDE OF EY AT X=12

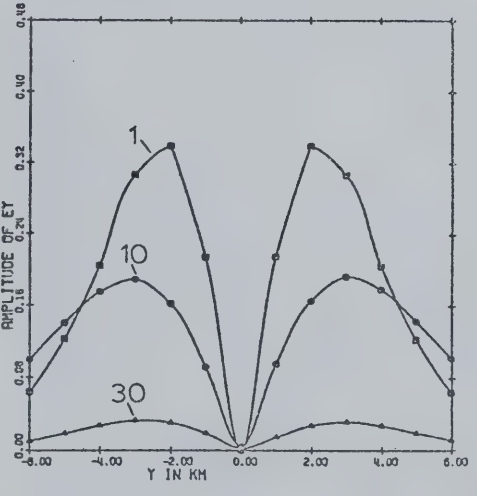

AMPLITUDE OF EY AT X=18

Fig. 18. Amplitude profiles of E_x, E_y, and E_z for the single island structure for one, ten, and thirty minute source periods.

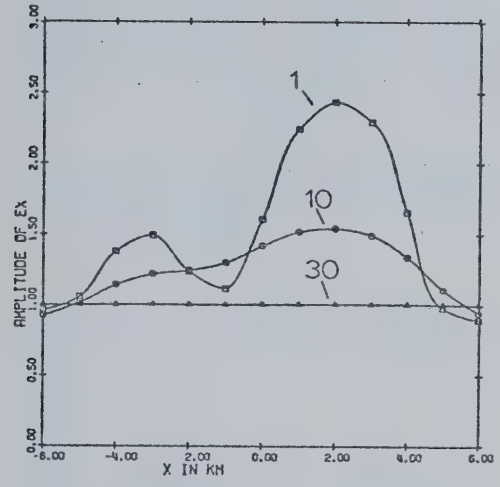

AMPLITUDE OF EX AT Y=13

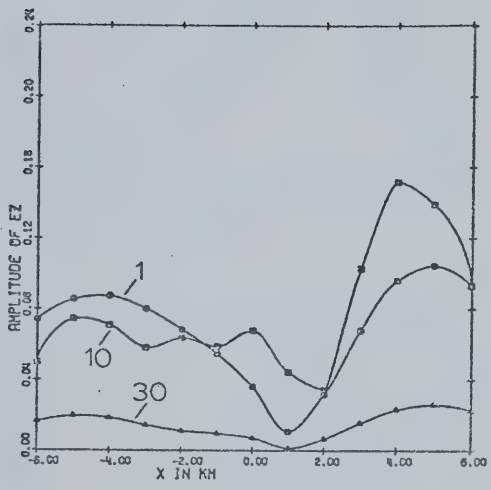

AMPLITUDE OF EZ AT Y=13

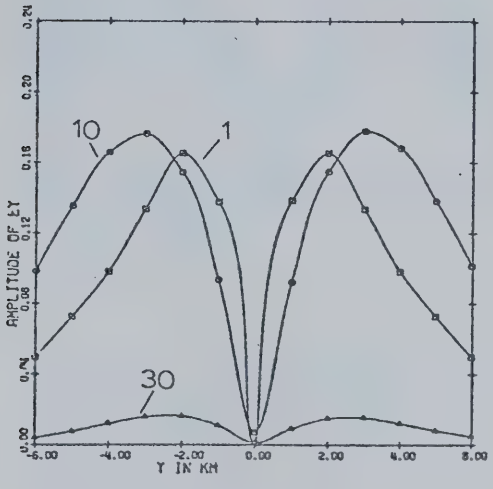

AMPLITUDE OF EY AT X=9

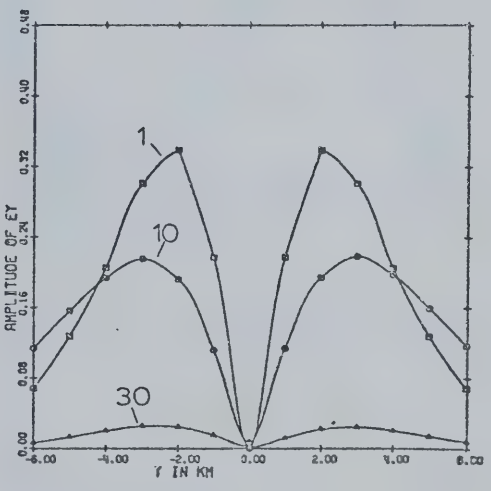

AMPLITUDE OF EY AT X=18

Fig. 19. Amplitude profiles of E_x, E_y, and E_z for the two-island structure for one, ten, and thirty minute source periods.

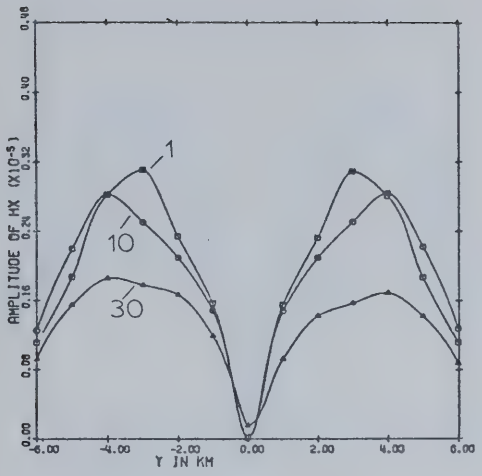

AMPLITUDE OF HX AT X=18

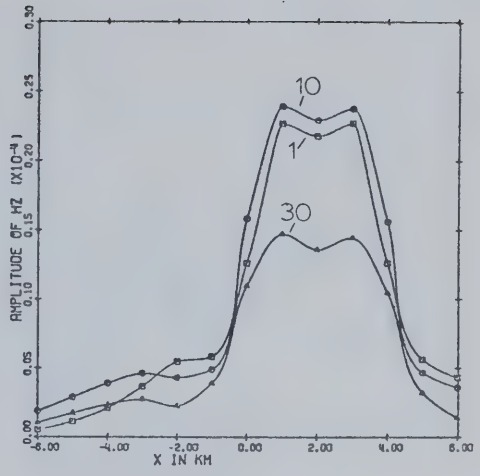

AMPLITUDE OF HZ AT Y=15

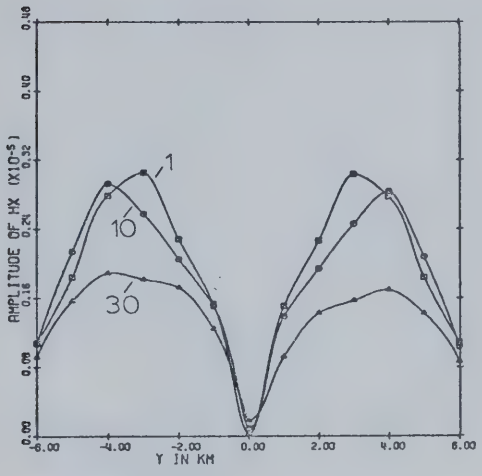

AMPLITUDE OF HX AT X=12

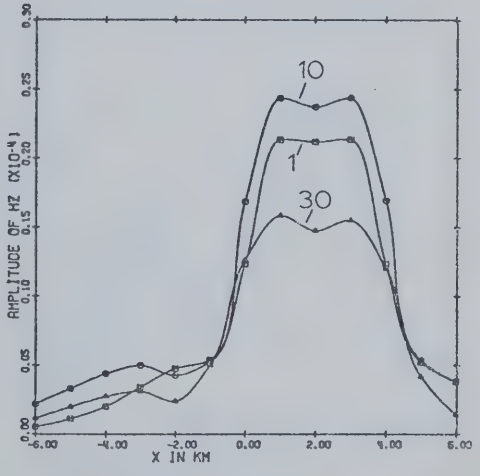

AMPLITUDE OF HZ AT Y=10

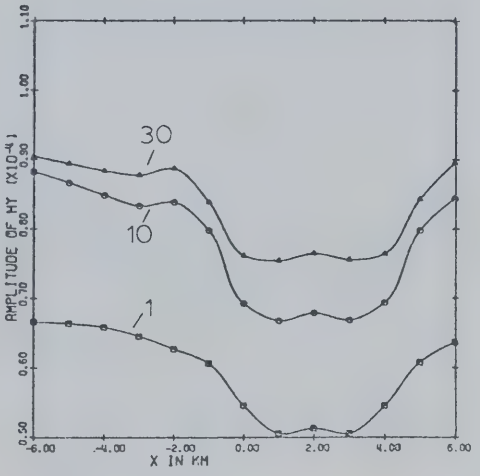

AMPLITUDE OF HY AT Y=13

Fig. 20. Amplitude profiles of H_x, H_y, and H_z for the single island structure for one, ten, and thirty minute source periods.

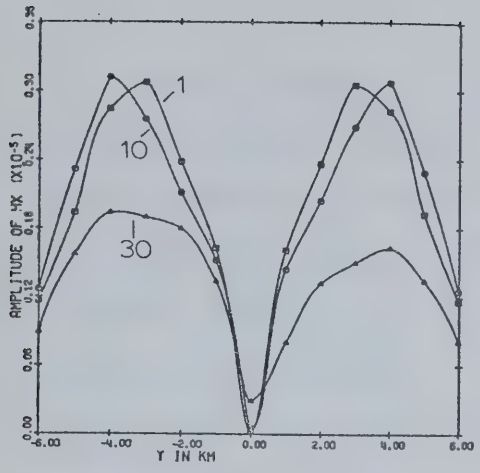

AMPLITUDE OF HX AT X=18

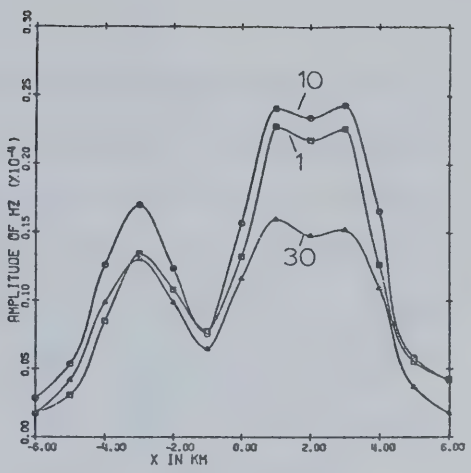

AMPLITUDE OF HZ AT Y=15

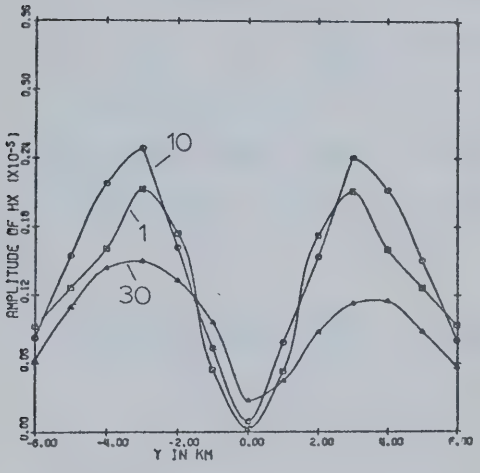

AMPLITUDE OF HX AT X=9

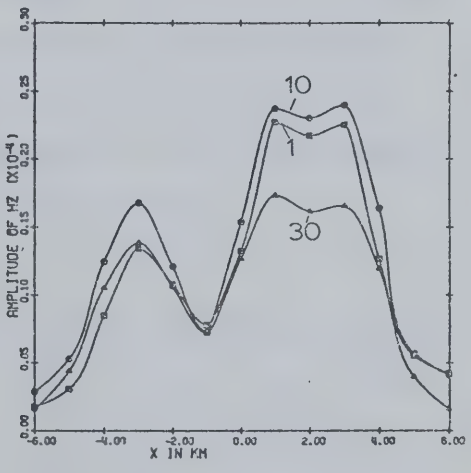

AMPLITUDE OF HZ AT Y=11

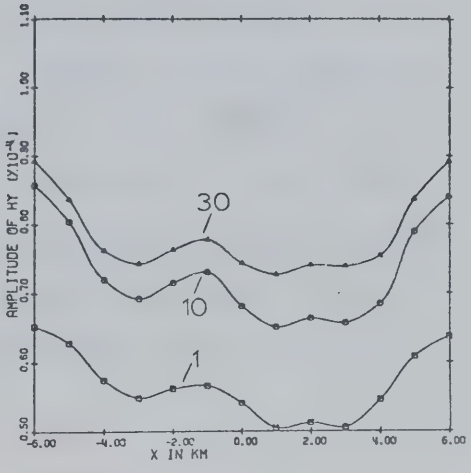

AMPLITUDE OF HY AT Y=13

Fig. 21. Amplitude profiles of H_x, H_y, and H_z for the two-island structure for one, ten, and thirty minute source periods.

As an example of the skin effect phenomenon, Figs. 18 to 21 may be examined. For the two-island structure, the values of $|E_x|$ along the profile Y = 13 show a much more distinct local maximum over the smaller island for a source period of one minute than is shown for a source period of ten minutes. At the outer boundaries of the grid, where the penetration of the fields by the island structure is assumed to be negligible, the value of E_x is normalized to 1.0 at the surface, with $E_y = E_z = 0$ there. We note from inspection of the profile values that the larger deviations of $|E_x|$ from 1.0 occur at higher frequencies where the shallow features of the island structures have a greater perturbation effect.

4.1.2.3 Amplitudes for a Source of Thirty Minute Period

For a source period of thirty minutes, Figs. 16 to 21 show that the effects of the smaller island on the $\underline{E}$ and $\underline{H}$ amplitudes are similar to the effects seen in the previous cases of one and ten minute periodicity.

As seen from the profile values, the amplitudes of E_x, E_y, and E_z are less at longer source periods. It must also be pointed out that variations in the $\underline{E}$ and $\underline{H}$ components are much less at the surface of the islands for a source of thirty minute period than they are for the shorter period sources, due to the fact that the

effect of the shallow structures is not as evident at longer periods.

4.1.2.4 Phase Comparisons

The signs of the vector components of $\underline{E}$ and $\underline{H}$, at a given time, are determined by the phase Φ. If we consider one component, such as E_x, then

$$E_x(x,y,z,t) = |E_x(x,y,z)|e^{i(\Phi+\omega t)} \quad . \qquad (4.9)$$

If there is a difference in phase of 180 degrees in E_x between different positions, then from the preceding expression for E_x it is seen that the observed field (i.e. $Re(E_x)$) for one position is opposite in sign to the observed field at the other position.

Phase profiles are shown in Figs. 22 to 25, and appropriate profiles are chosen to show sudden sign changes in the $\underline{E}$ and $\underline{H}$ components. These phase profiles must be interpreted with some degree of caution because the phase is determined by the argument of a complex number given by the ATAN2 function in Fortran IV. The argument of a complex number z is given by:

$$\Phi = \tan^{-1}\left(\frac{Im(z)}{Re(z)}\right) \quad , \text{ where } \quad -\pi \leq \Phi \leq \pi \quad . \qquad (4.10)$$

Hence, a small change in $\tan^{-1}\left(\frac{Im(z)}{Re(z)}\right)$ from 3.10 to 3.20

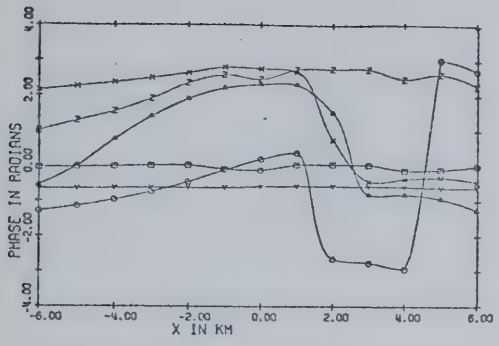

PHASE OF EX,EY,EZ,HX,HY,HZ AT Y=15

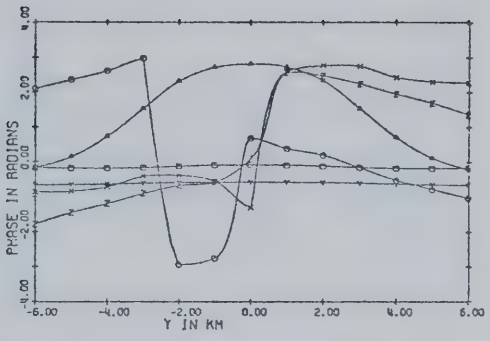

PHASE OF EX,EY,EZ,HX,HY,HZ AT X=13

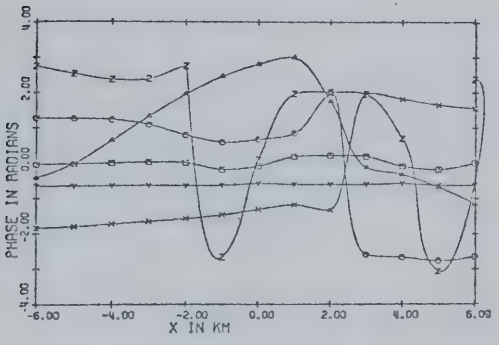

PHASE OF EX,EY,EZ,HX,HY,HZ AT Y=13

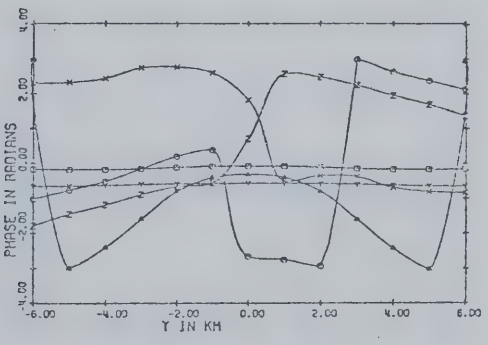

PHASE OF EX,EY,EZ,HX,HY,HZ AT X=17

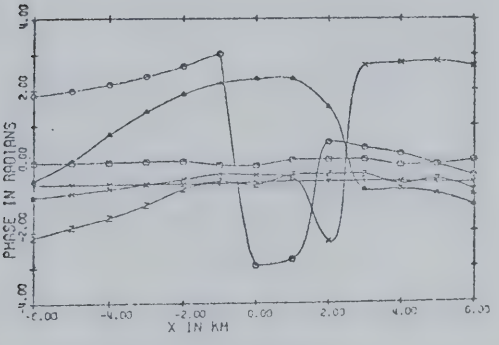

PHASE OF EX,EY,EZ,HX,HY,HZ AT Y=11

Fig.22. Phase profiles for the single island structure for a source period of one minute. Symbols used for phases: □, phase of E_x; ○, phase of E_y; Δ, phase of E_z; X, phase of H_x; Y, phase of H_y; Z, phase of H_z.

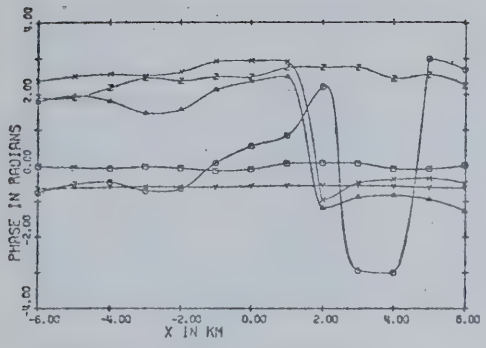

PHASE OF EX,EY,EZ,HX,HY,HZ AT Y=15

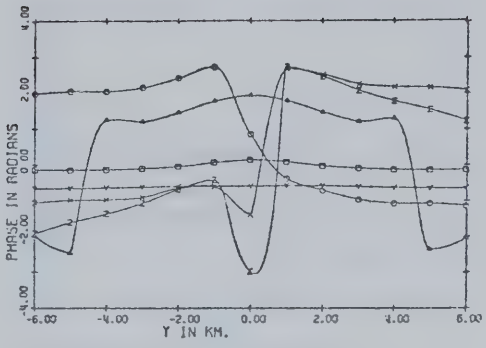

PHASE OF EX,EY,EZ,HX,HY,HZ AT X=10

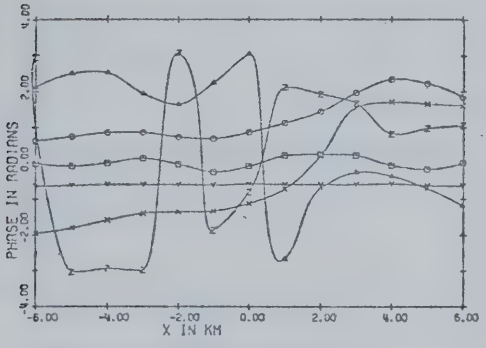

PHASE OF EX,EY,EZ,HX,HY,HZ AT Y=13

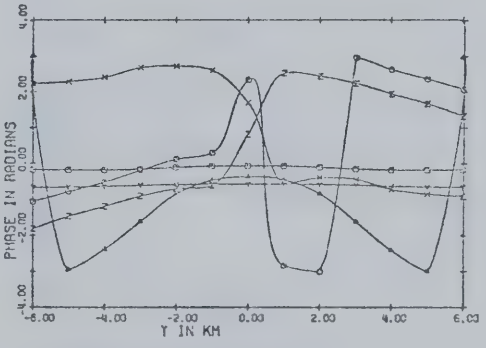

PHASE OF EX,EY,EZ,HX,HY,HZ AT X=17

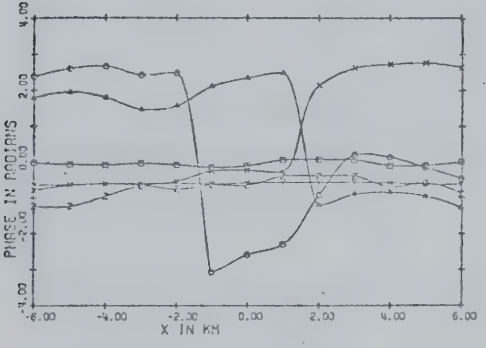

PHASE OF EX,EY,EZ,HX,HY,HZ AT Y=11

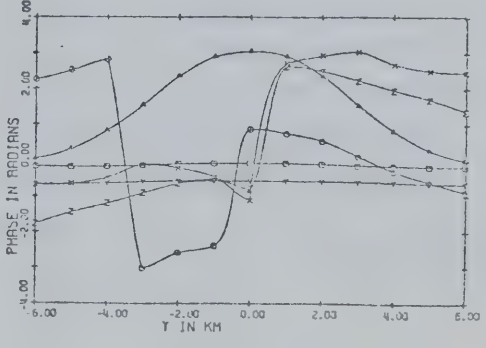

PHASE OF EX,EY,EZ,HX,HY,HZ AT X=13

Fig. 23. Phase profiles for the two island structure for a a source period of one minute. Symbols used for phases: □, phase of E_x; ○, phase of E_y; Δ, phase of E_z; X, phase of H_x; Y, phase of H_y; Z, phase of H_z.

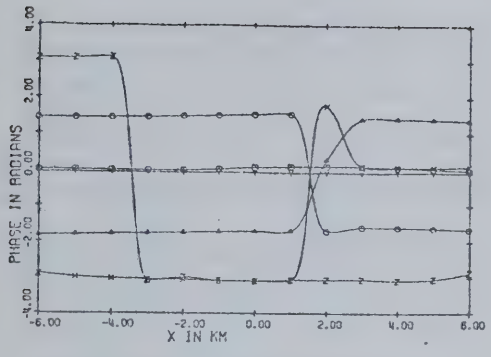

PHASE OF EX,EY,EZ,HX,HY,HZ AT Y=15

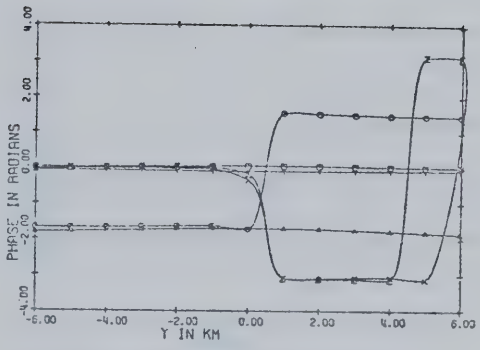

PHASE OF EX,EY,EZ,HX,HY,HZ AT X=13

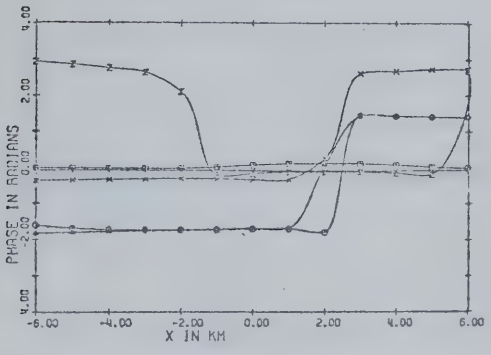

PHASE OF EX,EY,EZ,HX,HY,HZ AT Y=13

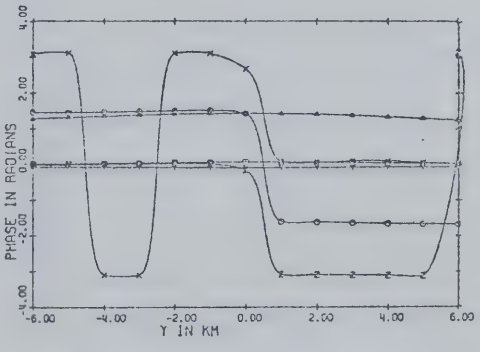

PHASE OF EX,EY,EZ,HX,HY,HZ AT X=17

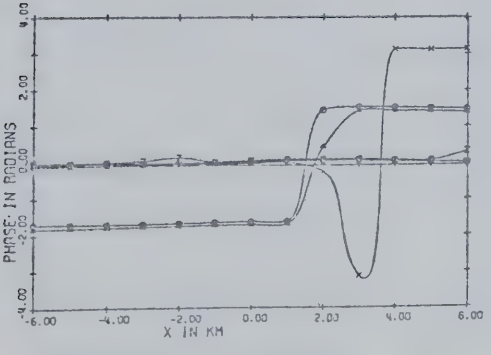

PHASE OF EX,EY,EZ,HX,HY,HZ AT Y=11

Fig. 24. Phase profiles for the single island structure for a source period of thirty minutes. Symbols used for phases: □, phase of E_x; ○, phase of E_y; Δ, phase of E_z; X, phase of H_x; Y, phase of H_y; Z, phase of H_z.

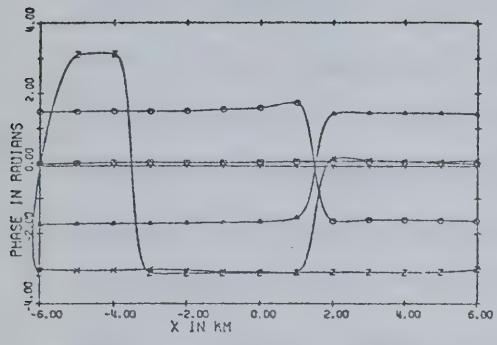

PHASE OF EX,EY,EZ,HX,HY,HZ AT Y=15

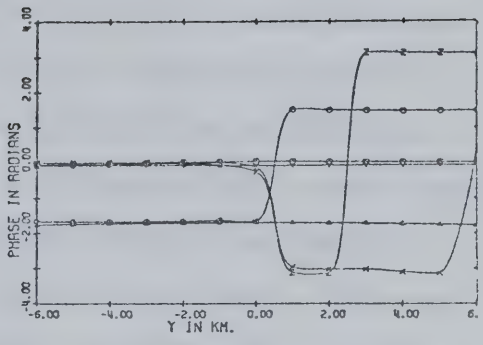

PHASE OF EX,EY,EZ,HX,HY,HZ AT X=10

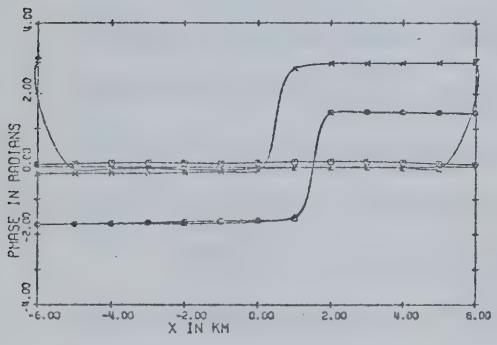

PHASE OF EX,EY,EZ,HX,HY,HZ AT Y=13

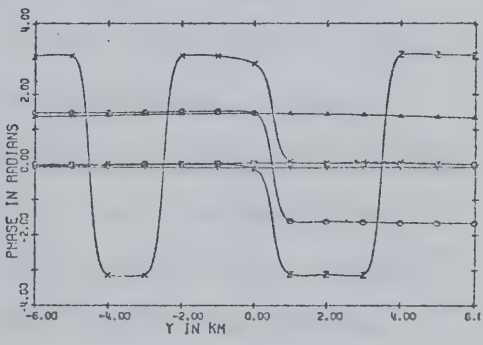

PHASE OF EX,EY,EZ,HX,HY,HZ AT X=17

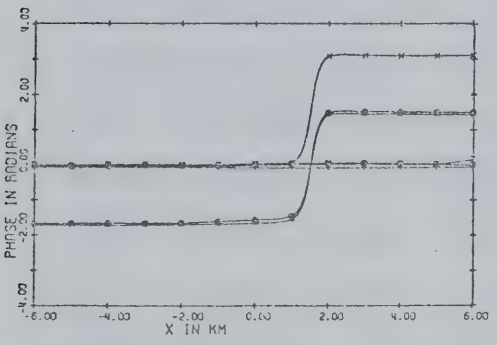

PHASE OF EX,EY,EZ,HX,HY,HZ AT Y=11

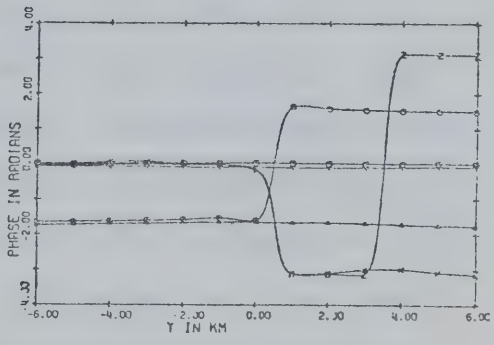

PHASE OF EX,EY,EZ,HX,HY,HZ AT X=13

Fig. 25. Phase profiles for the two-island structure for a source period of thirty minutes. Symbols used for phases: □, phase of E_x; ○, phase of E_y; Δ, phase of E_z; X, phase of H_x; Y, phase of H_y; Z, phase of H_z.

would result in a large jump in Φ from 3.10 radians to -3.08 radians when the argument is computed. Therefore, we must recognize jumps of about 2π in the phase profiles and realize that their cause is of no important physical significance. We must also realize that along profiles where the amplitudes of an $\underline{E}$ or $\underline{H}$ component are vanishingly small, the phase profiles of this component may exhibit sign changes which are of no great significance, but are due to the fact that our solutions are found by numerical methods and that the convergence factor is small but finite, giving small inherent errors. The smooth curve function used in the plotting program gives a double valued function at the end point of the profiles in a few cases, but this is not critical to the interpretation.

Consider initially the case of the single island. For all frequencies of the source, the Y = 13 profile in all figures shows no sudden changes in the phase of E_x or H_y. This implies that E_x and H_y, for a given time, have constant sign across the surface of the island(s). However, the phase of E_z undergoes a 180 degree phase change at the center of the large island, indicating a change in the sign of E_z there. This agrees with the behaviour of E_z predicted from Fig. 13(b). The direction of E_z just above the surface depends on the sign of the minute surface charges, and the sign of these charges depends on the vertical direction of subsurface currents.

The phase profile figures for source periods of 30 minutes are used in the subsequent discussions since these showed fewer 2π jumps than profiles at other frequencies. However, similar physical features are exhibited by phase profiles for the higher frequency cases. The profiles X = 13, X = 17, Y = 11 and Y = 15 of Fig. 24 all indicate that the components E_y and H_x undergo 180 degree phase changes at the center of the island for a thirty minute period. From these four profiles it can be seen that E_y and H_x will exhibit a "quadrature" behaviour in sign. In other words, E_y and H_x have opposite signs for adjacent quadrants centered about the middle of the larger island. Similar behaviour in the sign of E_y and H_x is given from the results of the other models considered. Fig. 13(a), which shows electric field lines in the x-y plane, predicts this behaviour in the sign of E_y. Application of the right hand rule to current flow in the y-z plane near the corners of the island agrees with such behaviour in the sign of H_x.

A similar application of the right hand rule to current flow in the x-y plane of Fig.13(a) will give a result which agrees with the sign of H_z predicted by our results. H_z is opposite in sign for the region Y > 13 as compared with the region Y < 13 for the coordinate system of Fig. 2. This sign difference is exhibited by the phase profiles X = 13 and X = 17 of Fig. 24. Mason

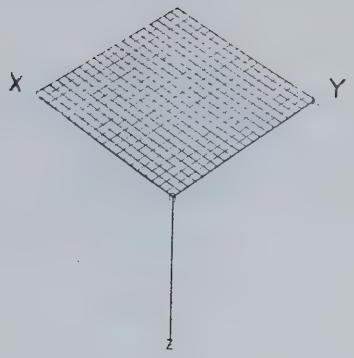

PHASE OF EX

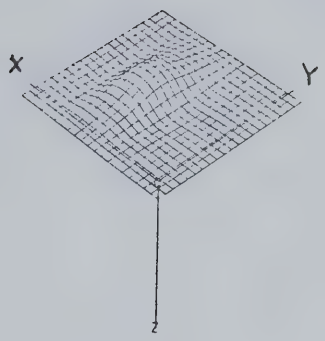

AMPLITUDE OF EX

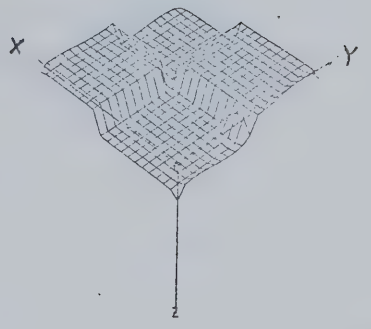

PHASE OF EY

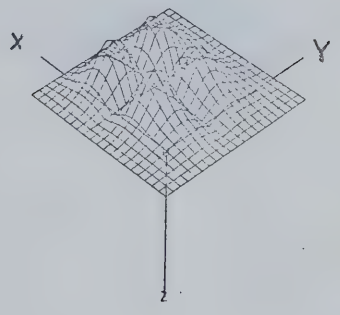

AMPLITUDE OF EY

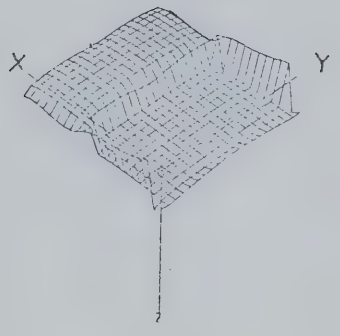

PHASE OF EZ

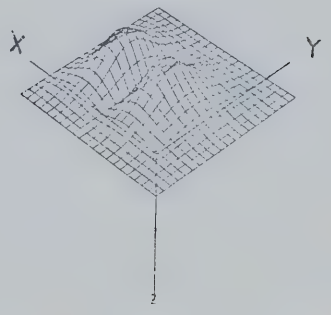

AMPLITUDE OF EZ

Fig. 26. Three-dimensional plots of the electric field component amplitudes and phases for the single island structure, for a period of thirty minutes. Inner 21 × 21 surface grid region is plotted.

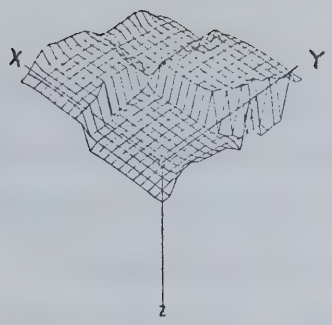

PHASE OF HX

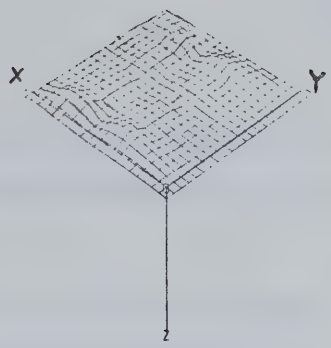

AMPLITUDE OF HX

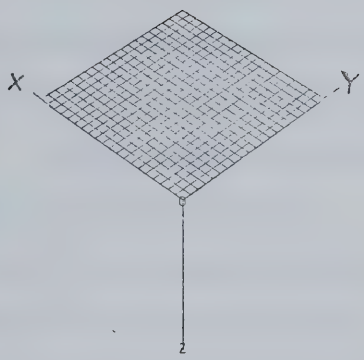

PHASE OF HY

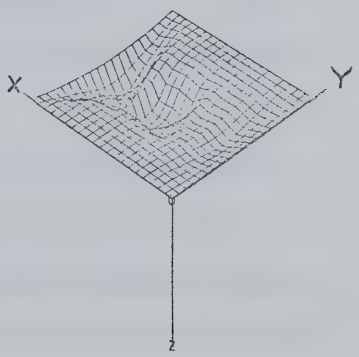

AMPLITUDE OF HY

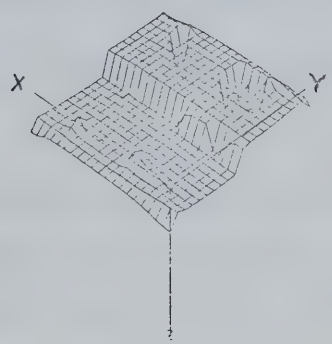

PHASE OF HZ

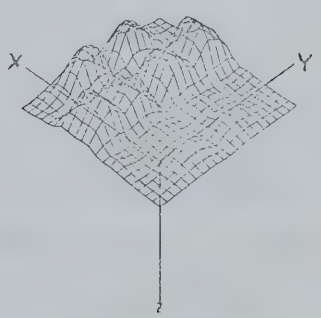

AMPLITUDE OF HZ

Fig. 27. Three-dimensional plots of the magnetic field component amplitudes and phases for the single island structure, for a period of thirty minutes. Inner 21 × 21 surface grid region is plotted.

(1963) noticed complete sign reversals in H_z values for stations 20 km apart from geomagnetic disturbances with a period of less than one hour.

The phase profiles of Fig. 25 for the two island structure show that sign changes in the components of $\underline{E}$ and $\underline{H}$ occur essentially in the same position as found in the single island structure at the same frequency (Fig. 24). In Fig. 25 an extra profile, X = 10, has been added to examine changes in Φ across the smaller island of the two island structure.

Three-dimensional graphs of the amplitudes and phases of all components of $\underline{E}$ and $\underline{H}$ are given for the case of the single island with a thirty minute source period in Figs. 26 and 27. These are of similar nature to those given by Jones and Pascoe (1972).

4.2 Application of the Three-Dimensional Method to a Coastline with a Nearby Island

4.2.1 Description of the Models

The perturbations of geomagnetic fields by two-dimensional coastline structures and three-dimensional island structures have so far been considered. In the present section the two-dimensional and three-dimensional methods are combined to model the effect of an island near a coastline. The model considered is that of a long

coastline of unlimited extent with a nearby island of limited extent. This structure is not purely two-dimensional throughout and therefore must be modeled by three-dimensional methods.

At a long distance from the three-dimensional island but in the direction of the coastline, the electric field is relatively undisturbed by the island and is parallel to the strike of the coastline. For this reason, we may use the solution of the two-dimensional E-polarization problem to provide boundary values for the three-dimensional model at the external boundaries of the grid.

The model used, shown in Fig. 28, is an island near a continental coastline with a shelf structure. The ocean-continental boundary strikes in the y direction. The conductivities used for the island and continental region, and for the ocean are given in Table 5 together with skin depths for these conductivities for a source period of thirty minutes. The model is described over a variable grid consisting of a $25 \times 25 \times 25$ array of points. Table 6 gives the dimensions of the variable grid used. The position of the surface of the conducting region is indicated by the vertical line in the z-direction dimensions. The inner uniform grid portion of the surface plane is shown in Fig. 29, along with the notation used for labelling the profiles. The surface contours and

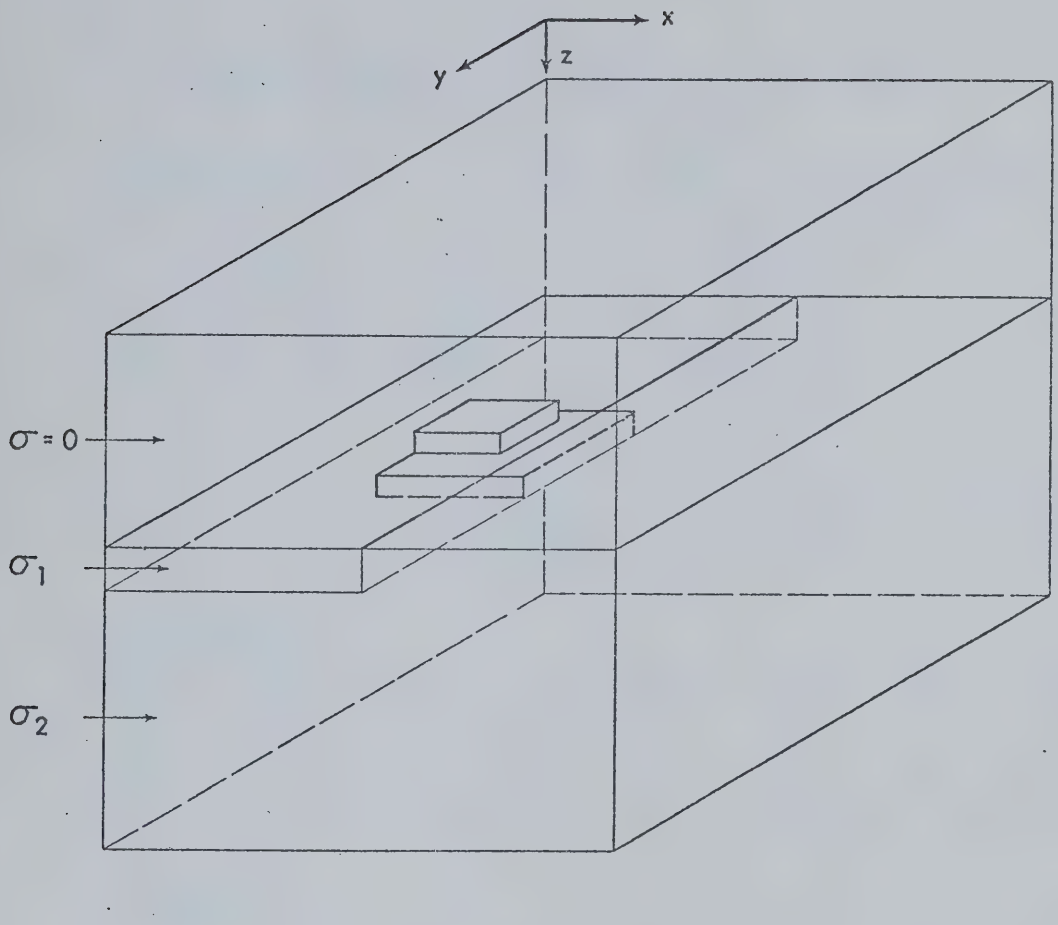

Fig. 28. A diagram of the three-dimensional model of an island near a coastline.

Table 5

Conductivities and skin depths for the model of an island near a coastline

Conductivities	Skin depths for 30 min period
$\sigma = 0$ (air)	infinite
$\sigma_1 = 4 \times 10^{-11}$ emu (ocean)	10.7 km
$\sigma_2 = 1 \times 10^{-14}$ emu (crust)	675.2 km

Table 6

Grid spacing for the model of an island near a coastline (in kilometers)

X direction

95.00	45.00	15.00	5.00	3.00	2.00	1.00	1.00
1.00	1.00	1.00	1.00	1.00	1.00	1.00	1.00
1.00	1.00	2.00	3.00	5.00	15.00	45.00	95.00

Y direction

95.00	45.00	15.00	5.00	3.00	2.00	1.00	1.00
1.00	1.00	1.00	1.00	1.00	1.00	1.00	1.00
1.00	1.00	2.00	3.00	5.00	15.00	45.00	95.00

Z direction

99.00	80.00	40.00	20.00	10.00	5.00	3.00	2.00
1.00 |	1.00	1.00	2.00	4.00	8.00	16.00	32.00
64.00	99.00	99.00	99.00	99.00	99.00	99.00	99.00

(The vertical line denotes the position of the surface plane.)

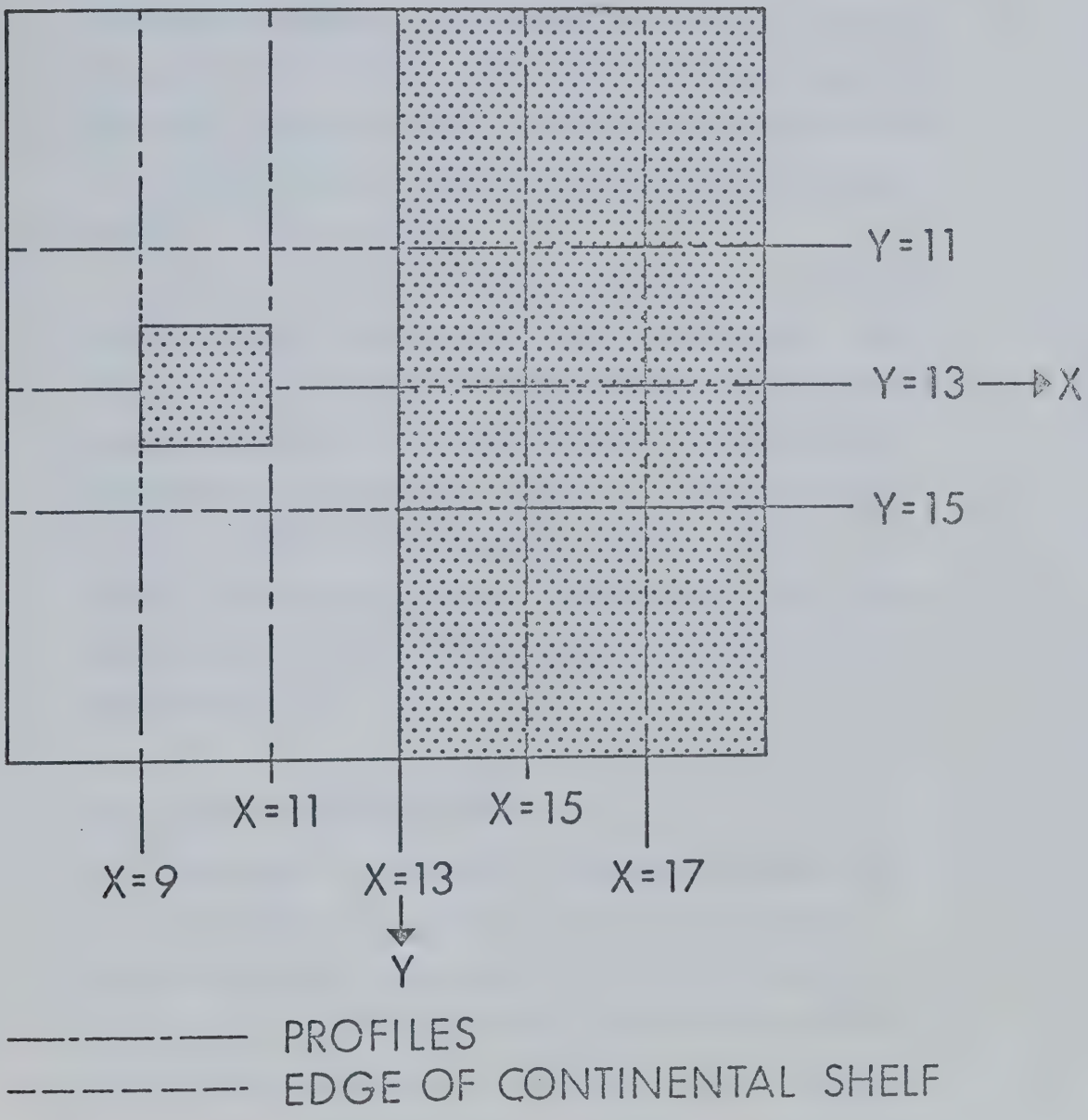

Fig. 29. The surface uniform grid region with some of the profiles considered for the model of an island near a coastline.

profiles, shown in later sections, are given for the uniform grid portion shown in this figure. The x-z plane perpendicular to the coastline at some distance from the island is shown in Fig. 30, and is the two-dimensional conductivity configuration which is solved to provide the boundary values for the three-dimensional island and coastline model. The electromagnetic fields are assumed to have a sinusoidal time variation with a period of thirty minutes.

Since we are considering a situation in which the electric field is polarized in the y direction, a solution for E_y satisfying the E-polarization equations and boundary conditions is determined for the coastline configuration illustrated in Fig. 30. This solution is used to provide the external boundary values for the $\underline{E}$ field. The $\underline{E}$-polarization solutions are also used to provide the initial internal values of $\underline{E}$ for the three-dimensional mesh.

4.2.2 Results and Discussion

Contours of the surface amplitudes for the six field components are given in Fig. 31, and profiles across the region illustrated in Fig. 29 are shown in Figs. 32 and 33. The amplitude contours and profiles of $|E_y|$ shown in Figs. 31 and 32 show that the island

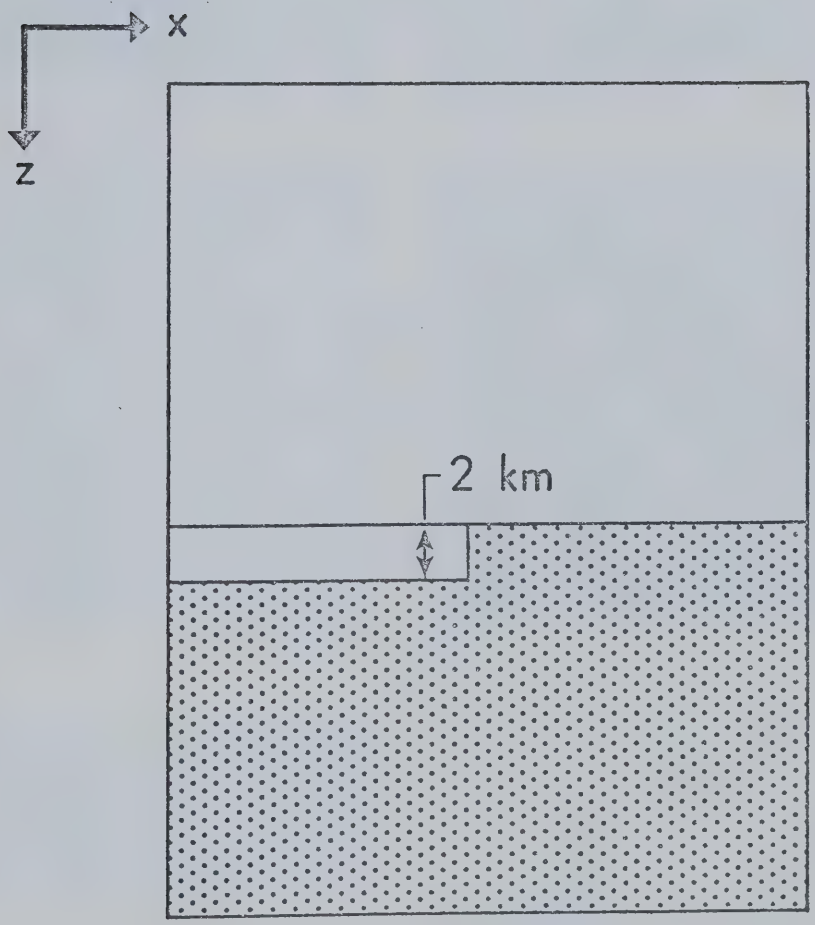

Fig. 30. The coastline configuration for the island-coastline model.

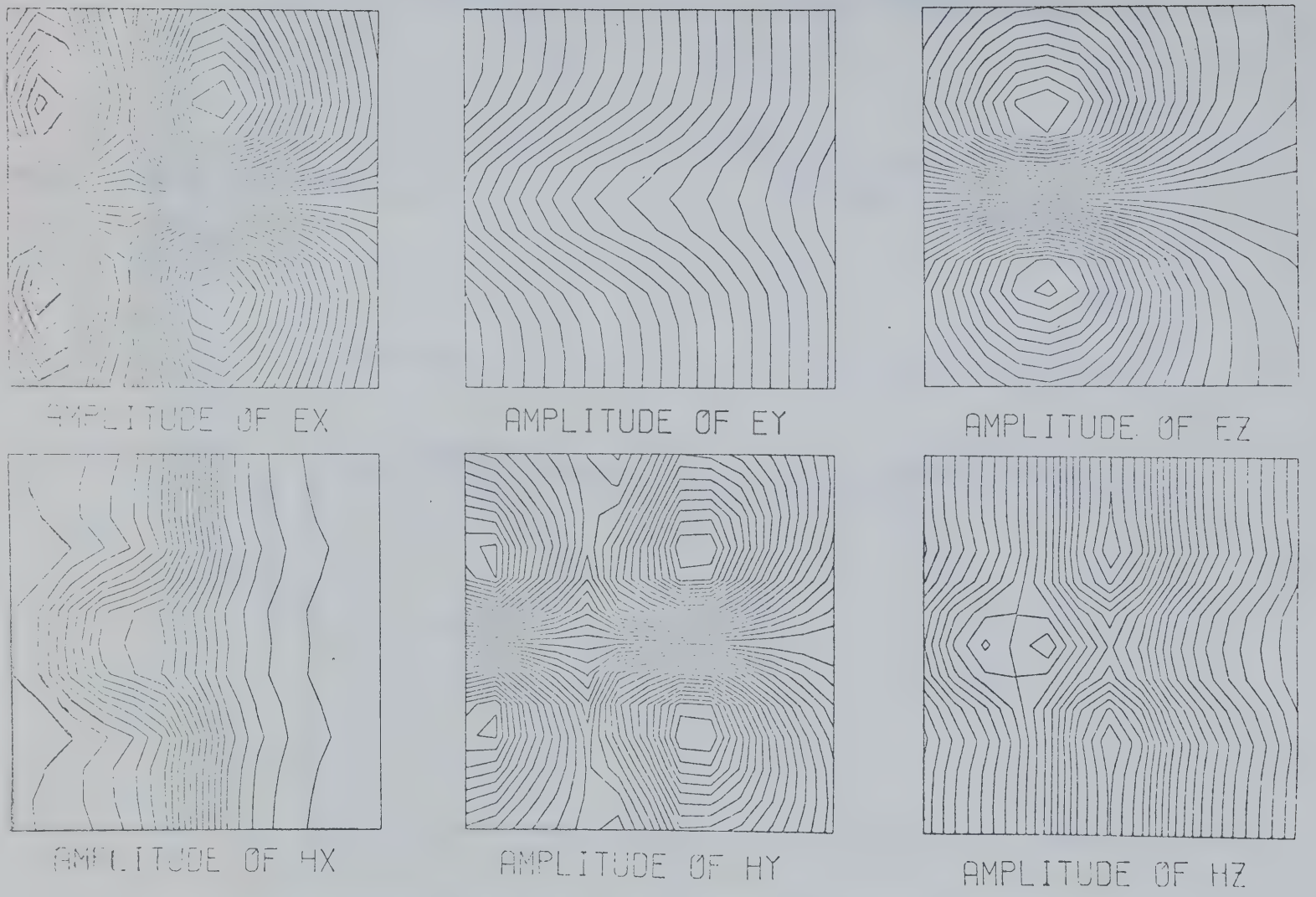

Fig. 31. The amplitude contours of the E and H components in the uniform grid region at the surface of the island-coastline model.

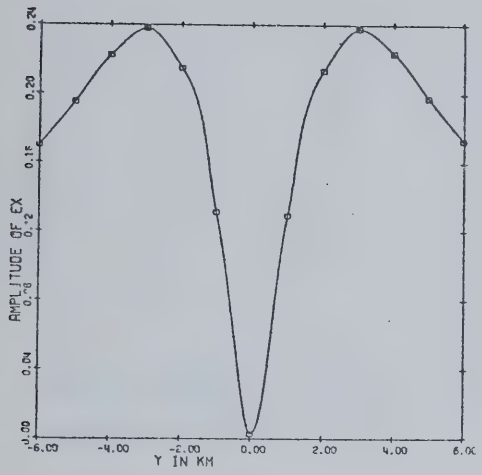

AMPLITUDE OF EX AT X=14

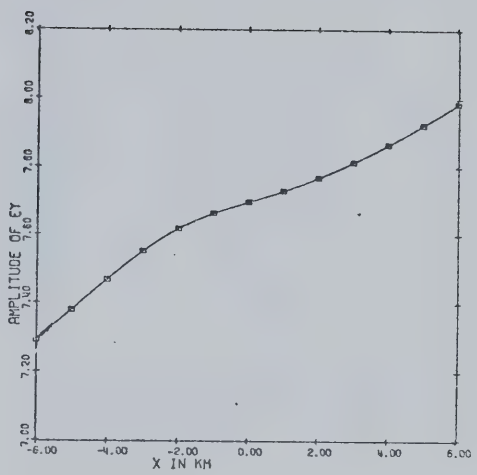

AMPLITUDE OF EY AT Y=13

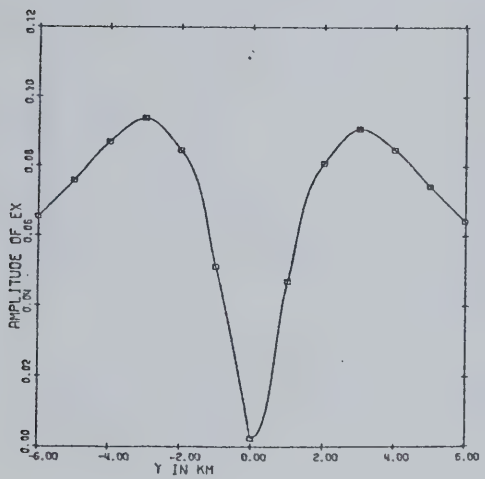

AMPLITUDE OF EX AT X=10

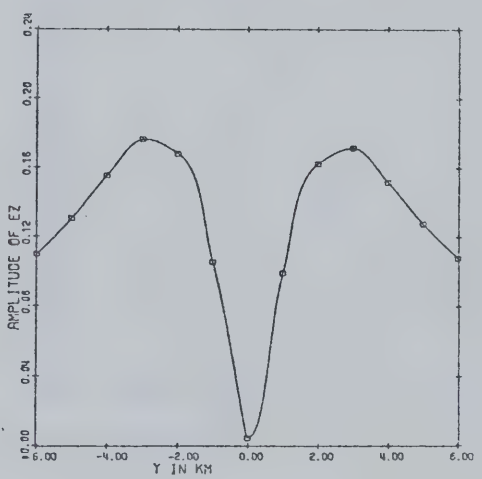

AMPLITUDE OF EZ AT X=11

Fig. 32. Surface amplitude profiles of E_x, E_y, and E_z for the island-coastline model.

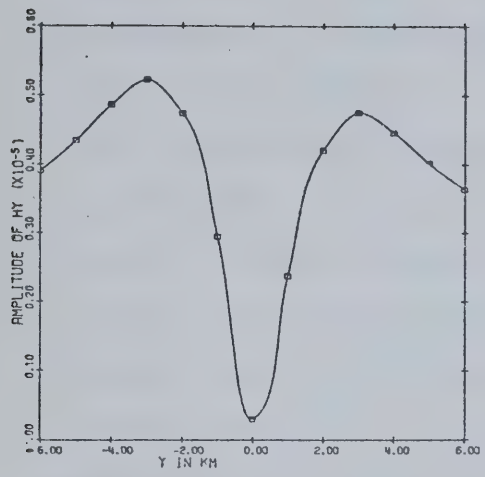

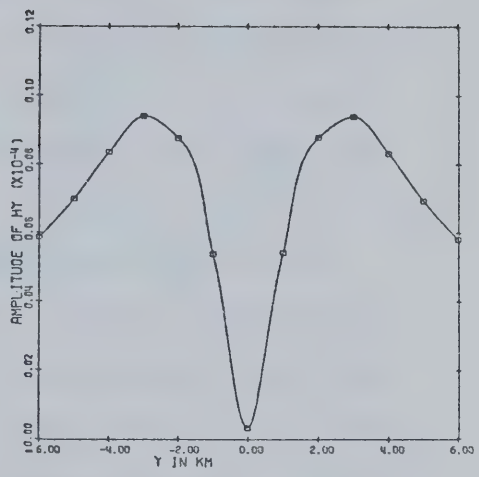

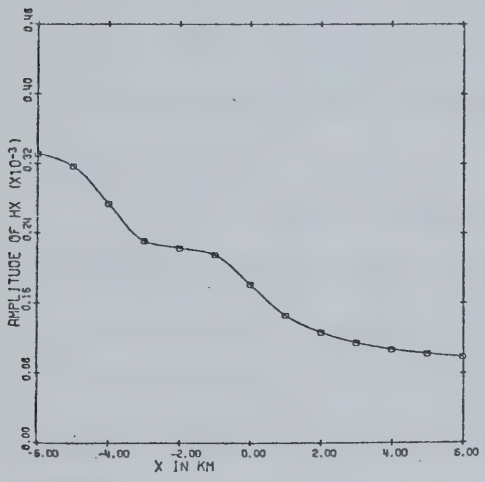

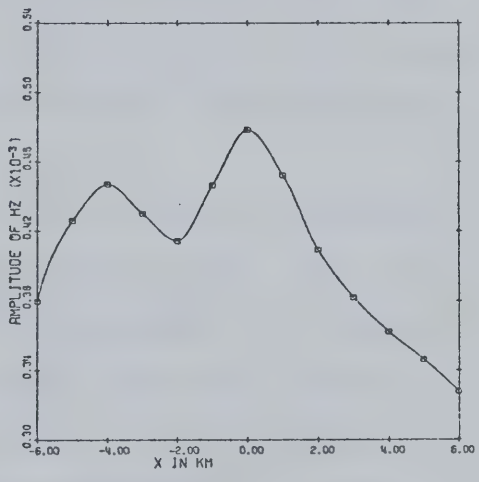

Fig. 33. Surface amplitude profiles of H_x, H_y, and H_z for the island-coastline model.

perturbs the E_y values associated with the coastline discontinuity. Over the island, the E_y amplitudes increase due to the presence of poorly conducting crustal material, causing contours of higher E_y values on the continent to be distorted toward the island. The E_x amplitude increases near the seaward corners of the island, indicating that at these positions electric currents are bending around the island. Three-dimensional graphs of the phase of the electric field components are given in Fig. 35. The graph for the phase of E_x exhibits shifts of π radians giving the expected sign differences in the E_x components at any given time for currents bending around the island. These sign changes are expected from examining the current flow diagram of Fig. 34(a).

Fig. 36 is a vector plot which shows the behaviour of the electric field vector near the island. This plot exaggerates the island effect as compared to the coastal effect since the vectors represent the vector sum of $E_x \times 0.10$ and $E_y \times 4.0$ for the time $t = 0$. The vector plot of the tangential component of $\underline{E}$ does not quite agree with the current flow diagram of Fig. 34(a), as seen from the $\underline{E}$ field vectors near the island and the coastline. The combined island and shelf structure acts as a crustal extension to the continent at a source

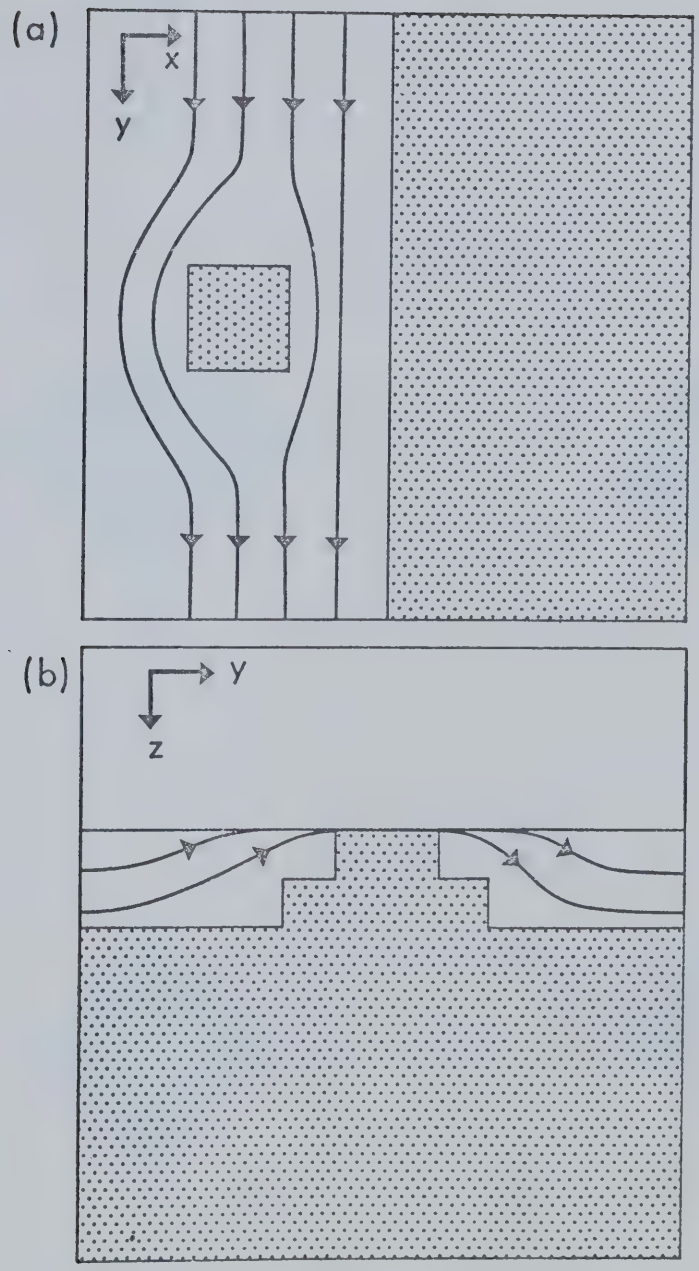

Fig. 34. Expected flow of electric currents for an island near a coastline. a) Current flow in the x-y plane b) Current flow in the y-z plane.

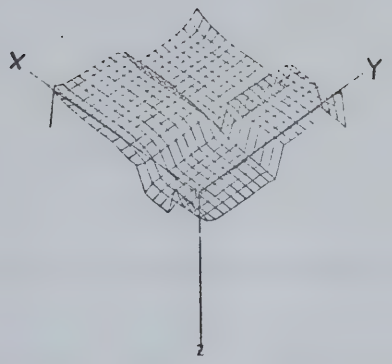

PHASE OF EX

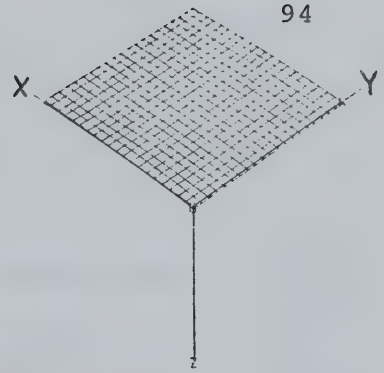

PHASE OF HX

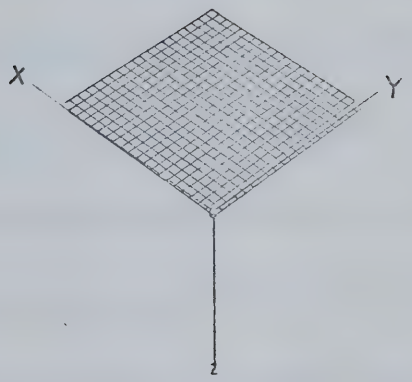

PHASE OF EY

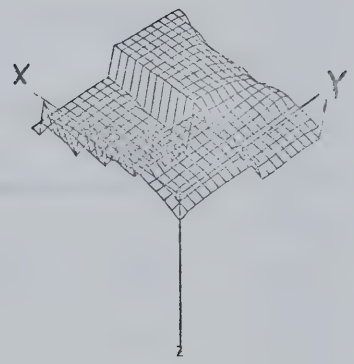

PHASE OF HY

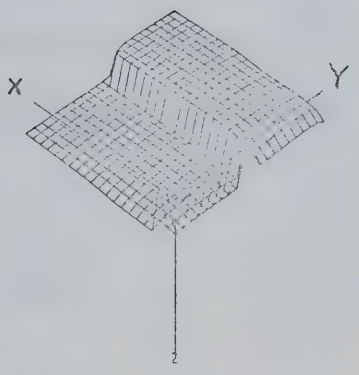

PHASE OF EZ

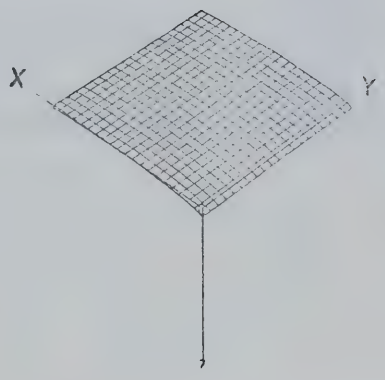

PHASE OF HZ

Fig. 35. Three-dimensional plots of the phases of the electric and magnetic fields for the island-coastline model.

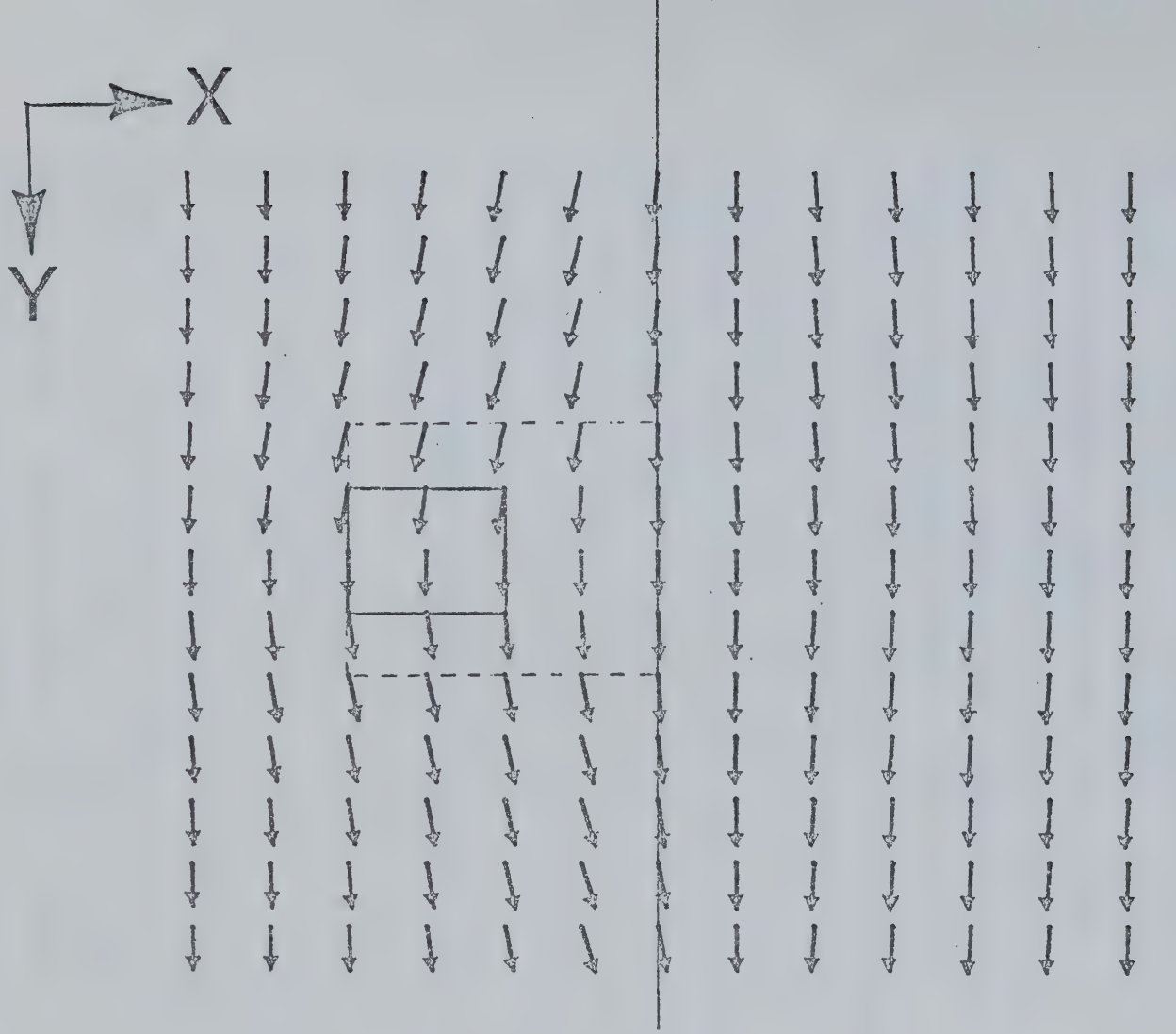

Fig. 36. Vector plot of the surface tangential electric field in the uniform grid region of the island-coastline model at time t=0. (Vectors represent vector sum of $E_x \times 4.0$ plus $E_y \times 0.10$. Dashed line represents shelf between the island and the coastline.)

period of thirty minutes, and the electric currents in the ocean tend to flow around the island and shelf structure. This vector plot was obtained from part of a programming package by Nyland and Lewis (1972).

From Figs. 31 and 32 it is observed that the largest values of $|E_z|$ occur where the magnitude of subsurface vertical currents as shown in Fig. 34(b) are greatest. The sign of E_z, given from the three-dimensional phase plots of Fig. 35, agrees with the expected sign of the subsurface currents. This behaviour in E_z is anticipated from the discussion of the effects of surface charges in the previous section. The correlation between the behaviour of oceanic electric currents and the vertical component of $\underline{E}$ at the surface supports the explanation by Price (1967).

The H_z component is found from the values of E_x and E_y by using

$$H_z = - \frac{1}{i\omega} \left(\frac{\partial E_y}{\partial x} - \frac{\partial E_x}{\partial y} \right) \quad . \tag{4.10}$$

The profiles and contours of H_z are shown in Figs. 31 and 33. A local maximum in H_z, shown in the Y = 13 profile of Fig. 33, is caused by the presence of the island. However, a larger increase in H_z is seen at the coastline. The dominant effect on H_z in the present

results is the coastal effect. The coastal effect on the vertical component of the magnetic field is caused by the concentrations of currents in the ocean, since only the crust and the ocean have been included in the model. In the actual situation, there is also a geomagnetic coastal effect caused by the mantle structure beneath the coastline.

The amplitude of H_x depends on current flow in the y-z plane. This current flow is less through the island and the continent, causing a decrease in the H_x component over these regions. This is shown in the amplitude contours and profiles of $|H_x|$ of Figs. 31 and 33.

The behaviour of H_y agrees with the application of the right hand rule to currents in the x-z plane. The amplitudes of H_y are shown in a contour plot in Fig. 31 and in two profiles in Fig. 33. The correct sign relationship between H_y components at any given time is shown by the three-dimensional phase plots which indicate phase differences of π radians where expected.

The values of $|E_y|$ are normalized to 1.0 on the far left hand side of the model shown in Fig. 30. All other values of the $\underline{E}$ and $\underline{H}$ components are scaled accordingly.

CHAPTER 5

SUGGESTIONS FOR FURTHER RESEARCH

Many of the techniques involved in analyzing geomagnetic perturbations by three-dimensional methods are in the development stage. Solutions have been given here for imbedded three-dimensional structures in a layered conducting half-space and also for imbedded three-dimensional structures which perturb an E-polarization field.

Numerical solutions for two-dimensional H-polarization fields have been developed by Jones and Pascoe (1971), and Pascoe and Jones (1972). Therefore, the fields for the two-dimensional coastal structures given previously may be solved for the H-polarization case. However, to apply the iterative technique of the three-dimensional perturbation method, initial values of $\underline{E}$ must be specified everywhere in the grid. In the H-polarization numerical method, values of $\underline{H}$ in a two-dimensional grid are calculated everywhere. However, if σ is taken as zero above the surface, then there is no obvious method of setting the $\underline{E}$ values above the surface. The problem arises in attempting to define the form of $\underline{E}$ across the surface boundary. The combined island-coastline problem should be investigated for the

case in which $\underline{H}$ is parallel to the coastline at a great distance from an island structure.

It would be valuable to compare the results from the three-dimensional numerical method with those of any analytical solutions which can be developed for similar models. For example, a comparison of results from the method presented here with results from the thin-sheet approximation method given by Price (1949) would be of considerable interest.

The two-dimensional perturbation method has been applied to actual geomagnetic data (Duba and Lilley (1972), Gough and Camfield (1972)). The three-dimensional numerical solution should also be applied to experimental data.

Parkinson (1964) analysed the effects of induced currents on coastal geomagnetic variations by considering the direction of tilt for the "preferred planes" of magnetic variations. A study of the behaviour of the Parkinson vectors for various island and coastline models would prove useful.

A uniform source has been assumed in this work. Recently, Hibbs (1972) has considered solutions of the two-dimensional problem for sources which are non-uniform. It would be worthwhile to consider three-dimensional problems for more generalized source configurations.

REFERENCES

Cagniard, L., 1953. Basic theory of the magneto-telluric method of geophysical prospecting. Geophysics 18, 605-635.

Camfield, P.A., Gough, D.I., and Porath, H., 1971. Magnetometer array studies in the Northwestern United States and Southwestern Canada. Geophys. J.R. Astr. Soc. 22, 201-221.

Camfield, P.A., and Gough, D.I., 1972. Anomalies in daily variation magnetic fields in Northwestern United States and Southwestern Canada. Submitted.

Coggon, J.H., 1971. Electromagnetic and electrical modeling by the finite element method. Geophysics 36, 132-155.

Cox, C. S., Filloux, J.H., and Larsen, J.C., 1970. Electromagnetic studies of ocean currents and electrical conductivity below the ocean floor: in The Sea, Vol. 4, Part I, edited by A.E. Maxwell, J. Wiley and Sons, pp. 637-693.

D'Erceville, D., and Kunetz, G., 1962. The effect of a fault on the Earth's natural electromagnetic field. Geophysics 27, 651-66.

Dosso, H.W., 1966. Analogue model measurements for electromagnetic variations near a coastline. Can. J. Earth Sci. 3, 917-936.

Duba, A., and Lilley, F.E.M., 1972. The effect of an ocean ridge on geomagnetic variations. Submitted.

Edwards, R.N., Law, L.K. and White, A., 1971. Geomagnetic variations in the British Isles and their relation to electrical currents in the ocean and shallow seas. Phil. Trans. Roy. Soc. London 270 (A 1204), 289-323.

Garland, G.D., 1971. Introduction to Geophysics, W.B. Saunders Co., p.212.

Gough, D.I., and Reitzel, J.S., 1969. Magnetic deep sounding and local conductivity anomalies: in The Application of Modern Physics to the Earth and Planetary Interiors, edited by S.K. Runcorn, Wiley Interscience, pp. 139-153.

Gough, D.I., and Camfield, P.A., 1972. Conductive structures under the Northern Rocky Mountains. Submitted.

Hibbs, R.D., 1972. A study of aperiodic, spatially time-varying two-dimensional sources in electromagnetic induction. M. Sc. thesis, Dept. of Physics, Univ. of Alberta.

Jackson, J.D., 1962. Classical Electrodynamics, John Wiley and Sons.

Jones, F.W., and Ainslie, B.A., 1972. The perturbation of alternating geomagnetic fields by discontinuities with high conductivity contrasts. Phys. Earth Planet. Int. In press.

Jones, F.W.,and Price, A.T., 1970. The perturbations of alternating geomagnetic fields by conductivity anomalies. Geophys. J.R. Astr. Soc. 20, 317-334.

Jones, F.W.,and Pascoe, L.J., 1971. A general computer program to determine the perturbation of alternating electric currents in a two-dimensional model of a region of uniform conductivity with an embedded inhomogeneity, Geophys. J.R. Astr. Soc. 24, 3-30.

Jones, F.W.,and Pascoe, L.J., 1972. The perturbation of alternating geomagnetic fields by three-dimensional conductivity inhomogeneities. Geophys. J.R. Astr. Soc. 27, 479-485.

Jones, F.W., 1972. Induction in laterally non-uniform conductors: theory and numerical models. Phys. Earth Planet. Int. Submitted.

Klein, D.P., 1971. Geomagnetic time-variations on Hawaii Island and mantle electrical conductivity. Trans. Amer. Geophys. Union 52, Abstract GP15, 824.

Lahiri, B.N., and Price, A.T., 1939. Electromagnetic induction in non-uniform conductors, and the determination of the conductivity of the Earth from terrestrial magnetic variations, Phil. Trans. Roy. Soc. London, A, 237, 509-540.

Lambert, A., and Caner, B., 1965. Geomagnetic depth sounding and the coast effect in Western Canada. Can. J. Earth Sci. 4, 797-814.

Latka, R., 1966. Modellrechnungen zur induktion im elektrisch leitfahigen untergrund. Zeitschrift fur Geophysik 32, 512-517.

Lines, L.R., Ainslie, B.A., and Jones, F.W., 1972. Investigation of the coastal effect by three numerical models. Submitted.

Lines, L.R., and Jones, F.W., 1972a. The perturbation of alternating geomagnetic fields by three-dimensional island structures. Geophys. J.R. Astr. Soc. In press.

Lines, L.R., and Jones, F.W., 1972b. The perturbation of alternating geomagnetic fields by an island near a coastline. Can. J. Earth Sci. In press.

Mann, J.E., 1970. A perturbation technique for solving boundary value problems arising in the electrodynamics of conducting bodies. Appl. Sic. Res. 22, 113-126.

Mason, R.G., 1963. Spatial dependence of the time variations of the geomagnetic field on Oahu, Hawaii. Trans. Am. Geophys. Union 44, 40.

Neves, A., 1957. The generalized magnetotelluric period. Ph.D. thesis. Dept. of Geol. and Geophys., M.I.T.

Nyland, E., and Lewis, L., 1972. Interactive manipulation of three-dimensional vector data. In preparation.

Parkinson, W.D., 1964. Conductivity anomalies in Australia and the ocean effect. J. Geomagn. Geoelect. 15, 222-226.

Pascoe, L.J., and Jones, F.W., 1972. Boundary conditions and calculation of surface values for the general two-dimensional electromagnetic induction problem. Geophys. J.R. Astr. Soc. 27, 179-193.

Patrick, F.W., and Bostick, F.X., 1969. Magnetotelluric modelling techniques. Tech. Rept. 59, Electronics Research Center, Univ. of Texas, Austin.

Porath, H., and Gough, D.I., 1971. Mantle conductive structures in the Western United States from magnetometer array studies. Geophys. J.R. Astr. Soc. 22, 261-275.

Price, A.T., 1949. The induction of electric currents in non-uniform thin sheets and shells. Quart. J. Mech. Appl. Math. 2, 283-310.

Price, A.T., 1950. Electromagnetic induction in a semi-infinite conductor with a plane boundary. Quart. J. Mech. Appl. Math. 3, 385-410.

Price, A.T., 1962. The theory of magnetotelluric fields when the source field is considered. J. Geophys. Res. 67, 1907-1918.

Price, A.T., 1964. A note on the interpretation of magnetic variations and magnetotelluric data. J. Geomagn. Geoelect. 15, 241-248.

Price, A.T., 1967. Electromagnetic induction within the Earth: in Physics of Geomagnetic Phenomena, Vol. 1, edited by S. Matsushita and W. Campbell, Academic Press, pp. 235-298.

Rankin, D., 1962. The magneto-telluric effect on a dike. Geophysics 27, 666-676.

Reddy, I.K. and Rankin, D., 1972. Magnetotelluric response of a two-dimensional sloping contact by the finite element method. Pure and Applied Geophysics. In press.

Rikitake, T., 1964. Outline of the anomaly of geomagnetic variations in Japan. J. Geomagn. Geoelect. 15, 181-184.

Rikitake, T., 1966. Electromagnetism and the Earth's Interior. Elsevier Publishing Co., pp. 286-288.

Roden, R.B., 1964. The effect of an ocean on magnetic diurnal variations. Geophys. J.R. Astr. Soc. 8, 375-388.

Schmucker, U., 1964. Anomalies of geomagnetic variations in the Southwestern United States. J. Geomagn. Geoelect. 15, 193-221.

Smith, G.D., 1969. Numerical Solution of Partial Differential Equations, Oxford Univ. Press.

Srivistava, S.P., 1966. Theory of the magneto-telluric method for a spherical conductor. Geophys. J.R. Astr. Soc. 11, 373-387.

Treumann, R., 1970. Three-dimensional analysis of the electromagnetic induction problem of magnetic variation and magnetotelluric sounding. Geomagn. and Aeronomy 10, 849-853.

Wait, J.R., 1954. On the relation between telluric currents and the Earth's magnetic field. Geophysics 19, 281-289.

Wait, J.R., 1962. On the propagation of v.l.f. and e.l.f. radio waves when the ionosphere is not sharply bounded. J. Res. Nat. Bur. Stand. 66D, 53-62.

Weaver, J.T., 1963. The electromagnetic field within a discontinuous conductor with reference to geomagnetic micropulsations near a coastline. Can. J. Phys. 41, 484-495.

Weaver, J.T. and Thomson, D.J., 1972. Induction in a non-uniform conducting half-space by an external line current. Geophys. J.R. Astr. Soc. 28, 163-185.

Wright, J.A., 1969. The magnetotelluric and geomagnetic response of two-dimensional structures. GAMMA (Inst. Geophysik Meteorogie Tech. Univ. Braunschweig) 1, 102S.